Measurement, Modeling, and Simulation of Bulk Viscoelasticity for Amorphous Polymers

by

Yuan-Jung (Dan) Chang

A dissertation submitted in partial fulfillment of

the requirements for the degree of

Doctor of Philosophy

(Department of Mechanical Engineering)

at the

UNIVERSITY OF WISCONSIN–MADISON

2023

Date of final oral examination: 06/14/2023
The dissertation is approved by the following members of the Final Oral Committee:
Tim A. Osswald, Professor, Mechanical Engineering
Lih-Sheng (Tom) Turng, Professor, Mechanical Engineering
Pavana Prabhakar, Associate Professor, Civil and Environmental Engineering
Alejandro Roldán-Alzate, Associate Professor, Mechanical Engineering
Lianyi Chen, Associate Professor, Mechanical Engineering

Abstract

Bulk viscoelasticity is not well studied and understood in the field of polymer processing. Its behavior in solid mechanics applications, such as time-dependent bulk modulus and time-dependent thermal expansion, was rarely considered but started to receive attention recently. Bulk viscosity (bulk viscoelasticity in fluid mechanics formulation) has been ignored in polymer processing for decades. Bulk viscosity could play an essential role in compressible polymer melts that undergo substantial volume changes caused by variations in temperature and mechanical pressure during fluid motion and solidification.

This study investigates the bulk viscosity of an amorphous polymer, Polystyrene (PS), through measurements, modeling, and implementation in an injection molding simulation. The results demonstrated that bulk viscosity can be derived from a cooling rate-controlled PVT (pressure-specific volume-temperature) measurement. A new PVTQ (pressure-specific volume-temperature-cooling rate) model was developed to obtain smooth and reliable bulk viscosity results. Furthermore, a Cross-WLF (William-Landel-Ferry)-Arrhenius model was found capable of describing the dependence of temperature, rate of volume change, and mechanical pressure on bulk viscosity.

Simulation results of cavity pressures and shrinkages are validated with experimental data in a 3-plate mold case (part size 300 x 100 x 3 mm^3). The results demonstrate that the effects of bulk viscosity reduced mechanical pressure variations during the packing stage in injection molding. However, the cavity pressure predicted by GNF (Generalized Newtonian Fluid) models with bulk viscosity drops too fast during the holding stage. The current GNF model can neither accurately describe isothermal pressurization (bulk creep) experiment data. A three-element-based constitutive model is proposed to describe bulk viscoelasticity in isobaric cooling and isothermal pressurization PVT (pressure-specific volume-temperature) measurements. This proposed model's predictions of cavity pressure, part weight, and shrinkage agree with the experiments and show significant improvement over the GNF model.

Acknowledgments

I would like to express my appreciation to my advisor, Professor Tim A. Osswald, for encouraging me to pursuing a PhD degree, having me into your research group, and guiding me my research and life. I also want to express my gratitude to the members of my dissertation committee: Prof. Lih-Sheng Turng, Prof. Pavana Prabhakar, Prof. Lianyi Chen, and Prof. Alejandro Roldán-Alzate, for providing their valuable feedback and suggestions.

I want to thank CoreTech System (Moldex3D) Co., Ltd. for their support, resources, and providing valuable experimental data. Grateful thanks are to Professor Rong-Yeu Chang for the help in inspiring and motivating me to explore this research topic. I would also like to acknowledge the contribution of coworkers in this company, especially Chen-Chieh Wang and De-Lung Lai for PVT measurements and Ting-Yu Cheng for injection molding experiment.

I want to thank all current and former members of the Polymer Engineering Center for the inviting environment and valuable discussions. In particular, John Emmanuelle Estela-García for constructive criticism of the manuscript.

Finally, I would like to thank my family for their unconditional support. Thanks to Lucy, Charlie, and Larry for accompanying me and having a great time together in Madison.

Table of Contents

List of Figures

List of Tables

List of Abbreviations

Abbreviation	Meaning
3D	Three-Dimensional
CTE	Coefficient of thermal expansion
iPP	Isotactic polypropylene
ISO	International Organization for Standardization
LDPE	Low-density polyethylene
MFI	Melt flow index
PMMA	Polymethyl methacrylate
PS	Polystyrene
PTFE	Polytetrafluoroethylene
PVC	Polyvinyl chloride
PVT	Pressure-specific volume-temperature
PVTQ	Pressure-specific volume-temperature-cooling rate
SN	Sensor
WLF	William-Landel-Ferry Model

List of Symbols

Symbol	Description
T_g	Glass transition temperature
T_m	Melting temperature
η_E	Elongational viscosity
η_s *or* η	Shear viscosity
μ_d	Bulk viscosity
E	Young's modulus
G	Shear modulus
K	Bulk modulus
$G(t)$	Relaxation modulus
ρ	Density
$\mathbf{u}$	Velocity vector
t	Time
$\boldsymbol{\pi}$	Total stress tensor
p	Hydrostatic pressure or equilibrium pressure.
$\mathbf{I}$	Second-order unit tensor
$\boldsymbol{\tau}$	Extra stress tensor
$\nabla\mathbf{u}$	Velocity gradient tensor
$\mathbf{g}$	Gravity acceleration vector

T	Temperature
k	Thermal conductivity
$\alpha \quad or \quad \alpha_v$	Volumetric CTE
$(\boldsymbol{\tau} : \nabla \mathbf{u})$	Viscous dissipation
τ_{ij}	Extra stress tensor
μ_{ijkl}	Fourth order viscosity tensor
ϕ	Scalar or vector variable
Γ	Diffusivity
Q_ϕ	Source term
n_c	Number of bounding faces of a control volume
$\mathbf{A}$	Sparse and diagonal-dominated matrix
$\mathbf{\Phi}$	Variable vector
$\mathbf{b}$	Vector source term
x	Position
$\Delta E \quad or \quad \Delta H_T$	Activation energy
R	Gas constant
σ	Mechanical pressure.

$\hat{v}$	Specific volume;
$\hat{v}_t$	Specific volume at the transition temperature
T_t	Transition temperature
Q	Cooling rate
α_m	Volumetric CTE in the molten state
α_s	Volumetric CTE in the solid state
ΔT	Control factor of the transition state
Q_{slow}	Slowest cooling rate from the experiment
$(T_t)_{slow}$	Transition temperature of the slowest cooling rate
a_{T_t} , b_{T_t}	Parameters to control pressure effect on $(T_t)_{slow}$
$(\hat{v}_t)_{slow}$	Transition temperature of the slowest cooling rate
$a_{\hat{v}_t}$, $b_{\hat{v}_t}$	Parameters to control pressure effect on $(\hat{v}_t)_{slow}$
$(\alpha_m)_{slow}$	Volumetric CTE at the melt state of the slowest cooling rate
α_{m0}, α_{m1}, λ_m, n_m	Parameters to control pressure effect on $(\alpha_m)_{slow}$
$(\alpha_s)_{slow}$	Volumetric CTE at the solid state of the slowest cooling rate
α_{s0}, α_{s1}, λ_s, n_s	Parameters to control pressure effect on $(\alpha_s)_{slow}$

q_{T_t}	Parameter to the control cooling rate effect on transition temperature
q_{α_m}	Parameter to control the cooling rate effect on volumetric CTE at the melt state
q_{α_s}	Parameter to control the cooling rate effect on volumetric CTE at the solid state
T_H	Extremely high temperature that cooling rate effect can be neglected.
Q_{eq}	Hypothetical equilibrium cooling rate
N	A number to adjust hypothetical equilibrium cooling rate
T^*	Solidifying temperature
τ^*	Characteristic stress
n	Power law index
a^*	Time–temperature shift factor
A_1 , $\tilde{A}_2$	Parameters of William-Landel-Ferry (WLF) model
D_2 , D_3	Parameters of William-Landel-Ferry (WLF) model
K_e	Bulk modulus derived from equilibrium PVT
B_e	Bulk compliance derived from equilibrium PVT
α_e	Volumetric CTE derived from equilibrium PVT
$\dot{\varepsilon}_V$	Volumetric strain rate

$\dot{T}$	Temperature change rate
$\dot{p}$	Pressure change rate
σ^0	Initial mechanical pressure
σ^1	New mechanical pressure after a time increment
Δt	Time increment
p^0	Initial equilibrium pressure
λ	Retardation time
T^0	Initial temperature
T^1	New temperature after a time increment
$p_r^{\ 0}$	Initial equilibrium pressure in the rubbery spring
p_r	Current equilibrium pressure in the rubbery spring
$(\mu_d)_r$	Bulk viscosity of the rubbery dashpot
λ_r	Retardation time in the rubbery portion
B_r	Bulk compliance of the rubbery spring
α_r	Volumetric CTE of the rubbery spring
B_g	Bulk compliance of the glassy spring
α_g	Volumetric CTE of the glassy spring

p_0	Equilibrium pressure at a previous time
$(\nabla \cdot \mathbf{u})_g$	Glassy portion of the volume change rate
$(\nabla \cdot \mathbf{u})_r$	Rubbery portion of the volume change rate
T_s	A temperature in solid state
f	Adjusting ratio for bulk compliances of the glassy spring
S_v	Volumetric shrinkage
$\hat{v}_c$	Specific volume at the end of cooling
$\hat{v}_r$	Specific volume at room temperature under atmospheric pressure

1 Introduction

1.1 Material

There are two main categories of polymeric materials: thermoplastics and thermosets. Thermoplastics are un-crosslinked and can be re-melted after solidification, while thermosets are crosslinked and cannot be re-melted.

Thermoplastics can be further divided into two classes: amorphous and semi-crystalline. As a thermoplastic polymer cools down, amorphous polymers remain random and disordered, but semi-crystalline polymers can form some regular alignments. The microstructure variation from molten state to solid state in thermoplastics can be shown in **Figure 1.1**.

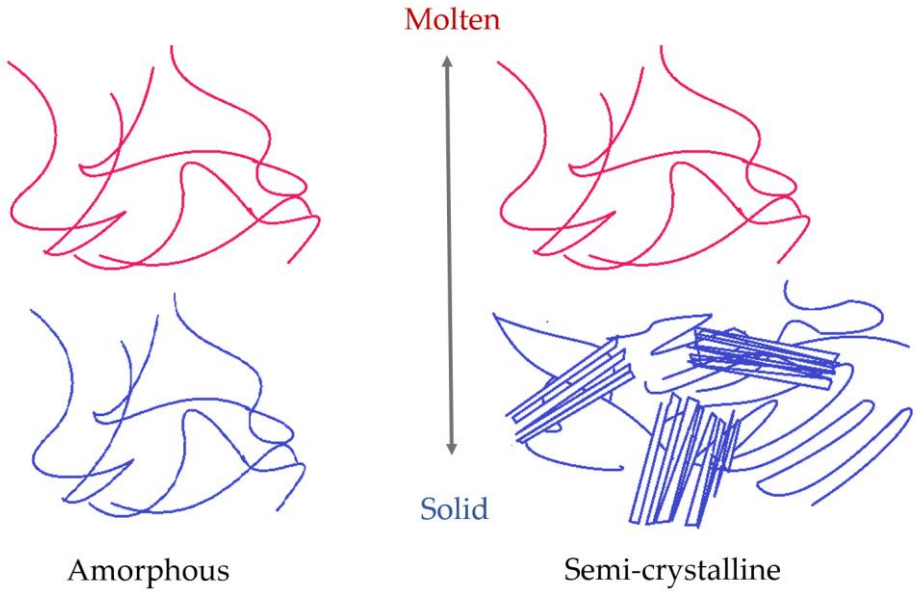

Figure 1.1 Microstructure of thermoplastics

The specific volume, representing density, is an important property for polymers. It is a function of pressure and temperature and can be plotted as a PVT (pressure-specific volume–temperature) diagram. The PVT diagram can show the significant difference between amorphous and semi-crystalline polymers. For semi-crystalline polymers, a sharp volume change (jump) can be observed as the temperature cools below melting point and the lamellar crystal structures are formed. On the other hand, amorphous polymers show the slope change in the PVT diagram but the volume changes gradually upon solidifying. Typical schematic PVT diagrams [1] for amorphous and semi-crystalline polymers are shown in **Figure 1.2**.

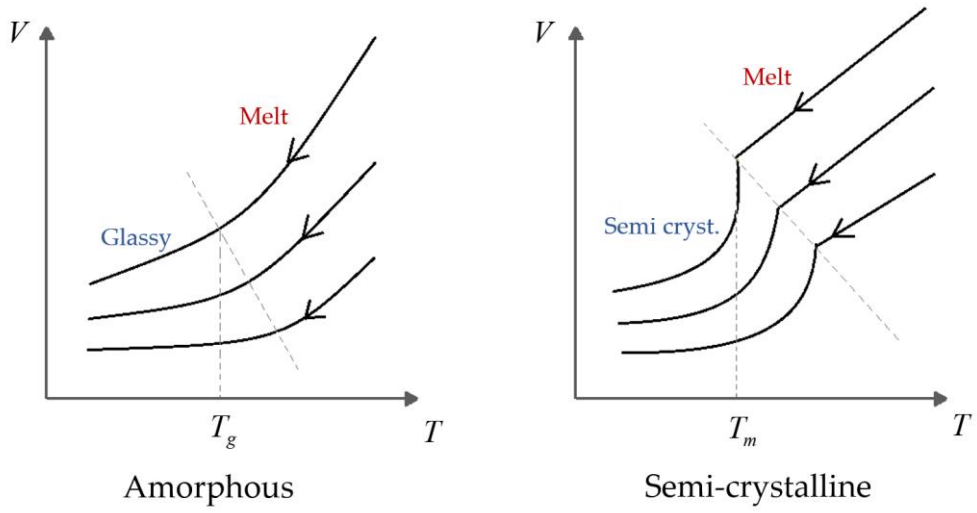

Figure 1.2 PVT diagram for amorphous and semi-crystalline polymers

Free volume in a polymer is defined as the volume that is not occupied by molecular chains and can be regarded as pores or voids between polymer chains.

As shown in **Figure 1.3**, free volume is larger and Brownian motion is rapid at high temperatures. Free volume collapses and reduces with lowering temperature. If the mobility of molecular chains is too small at low temperature, the free volume may keep in a similar extent. If the material undergoes high cooling rates, the collapse of voids cannot take place in time, resulting in an excess free volume. The change of excess free volume with time is the driving force behind physical aging. Free volume helps explain viscoelastic behavior, and it can be correlated to three stages: motion of chain ends, motion of side chains, and motion of the main chains.

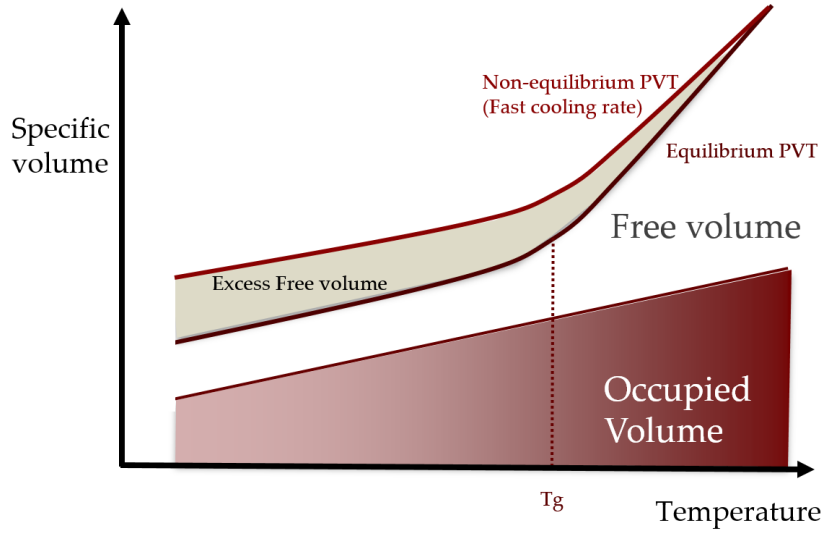

Figure 1.3 Schematic variation of specific volume around the glass transition temperature. (Including total specific volume, occupied volume, free volume, and excess free volume for an amorphous polymer)

Rheology is the field of science that studies material behavior in response to deformation. Polymers show a more interesting and complex response than

conventional Newtonian fluids. Polymer melts are viscoelastic, exhibiting a certain degree of solid-like elasticity or liquid-like viscosity under different circumstances. If the material behaved like an elastic solid, the stress was proportional to the strain, where modulus is a unit of measurement representing the proportional coefficient. On the other hand, if the material behaved like a viscous fluid, the stress was proportional to the strain rate, where viscosity represents the proportional coefficient. Material behavior in viscoelastic fluids, shown in **Figure 1.4**, can be differentiated into three categories according to the loading type: Elongational loading, Shear loading, Volumetric /Bulk loading (Compression).

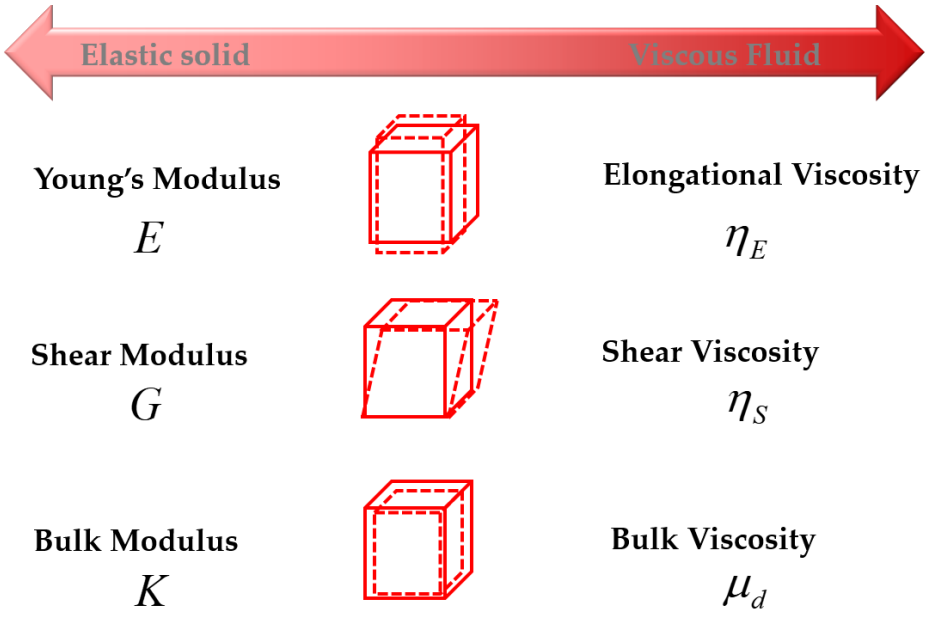

Figure 1.4 Material properties of viscoelastic fluids differentiated into three categories

1.2 Manufacturing

Injection molding is a cyclic polymer processing operation used to manufacture mass plastic products. More than one-third of thermoplastic materials nowadays are injection molded. The components of the injection molding machine are the plasticating/injection unit, clamping unit, and the mold [2], shown in **Figure 1.5**.

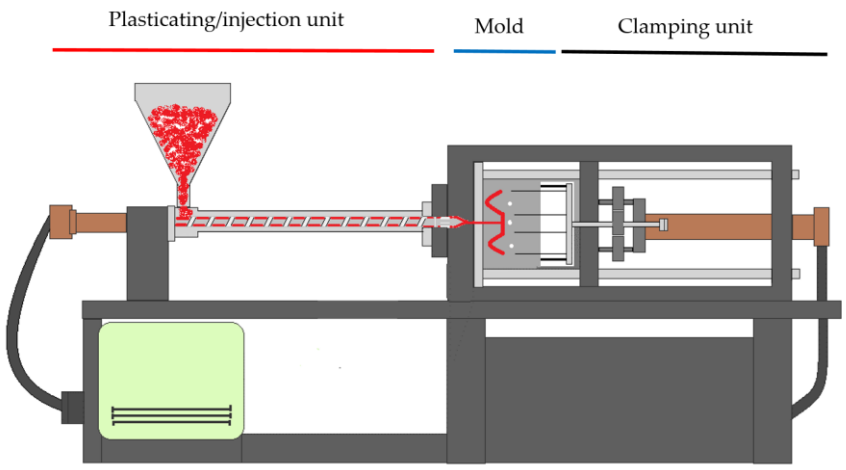

Figure 1.5 Schematic of an injection molding machine

The Injection molding cycle is shown in **Figure 1.6** [2]. First, the mold is closed by the clamping unit. The polymer melt is then injected into the mold cavity by moving the screw forward. Second, once the cavity is filled, the screw keeps moving by a small displacement to provide a higher packing pressure and then maintain a holding pressure to compensate for the volumetric shrinkage. Third, while the material keeps cooling down and solidifying in the mold, the screw starts to turn and move backward to add and plasticize new

materials, preparing for the next shot. Last, after the part in the mold is sufficiently cool, the mold opens and the part is ejected.

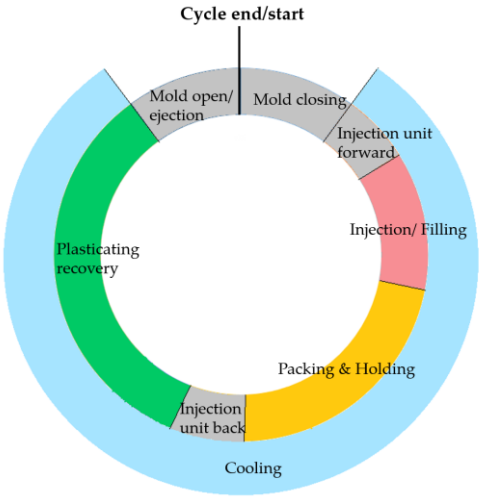

Figure 1.6 Injection molding cycle

1.3 Modeling and Simulation

There are three sets of governing equations that can be used to simulate the polymer melts, they are conservation of mass, momentum, and energy as follows:

$$\nabla \cdot \mathbf{u} = -\frac{1}{\rho}\frac{D\rho}{Dt} \tag{1.1}$$

$$\frac{\partial}{\partial t}(\rho \mathbf{u}) + \nabla \cdot (\rho \mathbf{u}\mathbf{u} - \boldsymbol{\pi}) = \rho \mathbf{g} \tag{1.2}$$

$$\rho C_p \left(\frac{\partial T}{\partial t} + \mathbf{u} \cdot \nabla T \right) = \nabla \cdot (k \nabla T) + \alpha T \frac{Dp}{Dt} + (\boldsymbol{\tau} : \nabla \mathbf{u}) \tag{1.3}$$

where ρ represents the density; $\mathbf{u}$ represents the velocity vector; t represents the time; $\boldsymbol{\pi}$ represents the total stress tensor, which consist of hydrostatic $-p\mathbf{I}$ and a deviatoric $\boldsymbol{\tau}$ portions; $\nabla \mathbf{u}$ represents the velocity

gradient tensor; $\mathbf{g}$ represents the gravity acceleration vector; C_p represents the specific heat; T represents the temperature; k represents the thermal conductivity; α represents volumetric CTE (coefficient of thermal expansion); and $(\boldsymbol{\tau}:\nabla\mathbf{u})$ represents the viscous dissipation.

There are several choices for constitutive models to describe the total stress tensor and extra stress tensor of polymer melts. If viscosity is considered as anisotropic, a form is given by

$$\tau_{ij} = \mu_{ijkl} \frac{\partial u_k}{\partial x_l} \tag{1.4}$$

where a fourth order viscosity tensor μ_{ijkl} with 81 coefficients is used. However, it is not easy to determine all coefficients of the anisotropic viscosity tensor and it is very difficult to converge in numerical simulations.

Generalized Newtonian Fluid is a common constitutive model to be used in injection molding simulation. This model assumes the fluid to be isotropic and no preferred direction, the total stress tensor is given by:

$$\boldsymbol{\pi} = -p\mathbf{I} + \left(\mu_d - \frac{2}{3}\eta\right)(\nabla\cdot\mathbf{u})\mathbf{I} + \eta\left(\nabla\mathbf{u} + (\nabla\mathbf{u})^T\right) \tag{1.5}$$

where p represents the hydrostatic pressure; $\nabla\cdot\mathbf{u}$ represents the divergence of the velocity vector, which describes the rate of volume change; η represents the shear viscosity, which describes the resistance to changes in shape; μ_d

represents the bulk viscosity, which describes the resistance to changes of volume.

A numerical approximation is needed to solve the governing equations and give numerical predictions. Finite volume is a common method used in computational fluid dynamics applications. This method is extended from the finite difference method and it can be applied to non-orthogonal grids. The spatial domain is subdivided into non-overlapping finite volumes or cells. The conservations of mass, momentum, and energy are then discretized as the following generic approach:

$$\frac{\partial}{\partial t}\left(\rho\phi\right)+\nabla\cdot\left(\rho\mathbf{u}\phi\right)-\nabla\cdot\left(\Gamma\nabla\phi\right)=Q_{\phi} \tag{1.6}$$

where ϕ can be a scalar or vector variable, Γ is the diffusivity, and Q_{ϕ} is the source term to take care of all other terms that cannot be discretized as the convection and diffusion terms. The governing equations to be solved can be casted in to these four terms: unsteady, convection, diffusion, and source terms.

Using Gauss divergence theorem to integrate the equation over the control volume to give the following form:

$$\int_{V}\frac{\partial}{\partial t}\left(\rho\phi\right)dV+\sum_{j=1}^{n_c}\int_{A_j}\left(\rho\mathbf{u}\phi-\Gamma\nabla\phi\right)=\int_{V}Q_{\phi}dV \tag{1.7}$$

where n_c is the number of bounding faces of a control volume (cell).

Summation of all the convection and diffusion fluxes in and out the faces will be balanced with the unsteady and source terms.

The final algebraic equation can be obtained in this form:

$$\mathbf{A\Phi = b} \tag{1.8}$$

where $\mathbf{A}$ is a sparse and diagonal-dominated matrix. $\mathbf{\Phi}$ is the variable vector, and $\mathbf{b}$ is the vector source term. The iterative methods can be used to solve this discretized algebraic equation.

An injection molding simulation has three stages [3]: pre-processing, computation, and post-processing. **Pre-processing** stage is to prepare the geometrical model, build a computational mesh, and provide the necessary information and settings before executing the simulation. **Computing** stage may cost a few minutes to a few days, depending on the different simulation goals and numerical approaches. **Post-processing** stage is to interpret the results; this requires experience and educated knowledge to get more insight from the simulation results. Depending on the goal of simulation, the model in pre-processing may include the whole molding system (parts, runners, cooling channels). Meshing is to subdivide the model into numerous cells with several element types, such as a tetrahedron, prism, hexahedron, etc. Meshing may take considerable time if a user chooses to build a hybrid mesh manually. Nowadays,

automatic meshing is approachable for some applications. Materials' rheological properties, which are essential for an accurate simulation, should be collected and well put in before the analysis. Process conditions such as melt temperature, mold temperature, flow rate profile, VP switch-over point, packing time, packing pressure profile and cooling time are also critical inputs for a simulation.

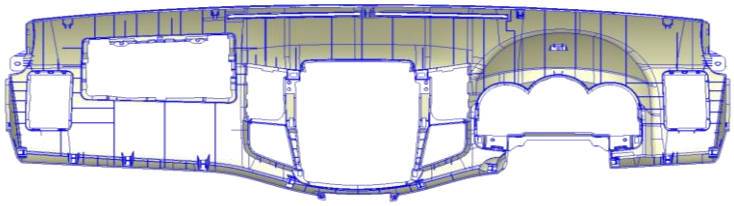

(a) Geometry model (Pre-processing)

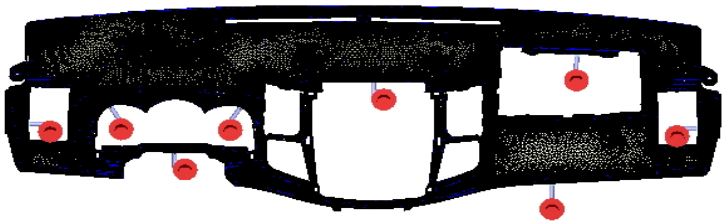

(b) Meshing (Pre-processing)

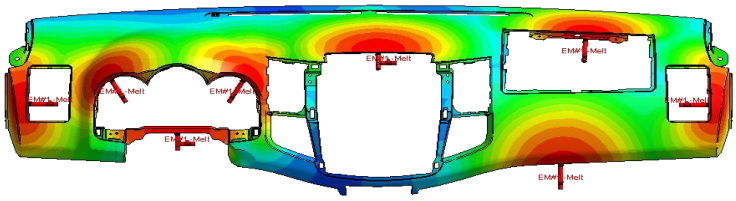

(c) Analysis result (Post-processing)

Figure 1.7 Injection molding Simulation

(Courtesy CoreTech System Co., Ltd.)

1.4 Motivation and Objectives

A typical pressure variation versus time at different locations (nozzle, a point close to the gate, and a point at the far end of the cavity) is shown in **Figure 1.8**. During the filling stage, the nozzle pressure is increased to provide the driving force to inject the polymer melt into the cavity. During the packing and holding stage, a high pressure in the nozzle is maintained in order to make the cavity pressure higher enough thus reducing the shrinkage. In real world experiments or manufacturing, it is often notice that cavity pressure cannot be raised to the high value that is ideally expected. At the beginning of packing, the pressure drops in the runner (between the nozzle and the gate) and cavity (between the gate and the far end of the cavity) are significantly higher than expected. The cavity pressures change slowly and maintain higher values during packing.

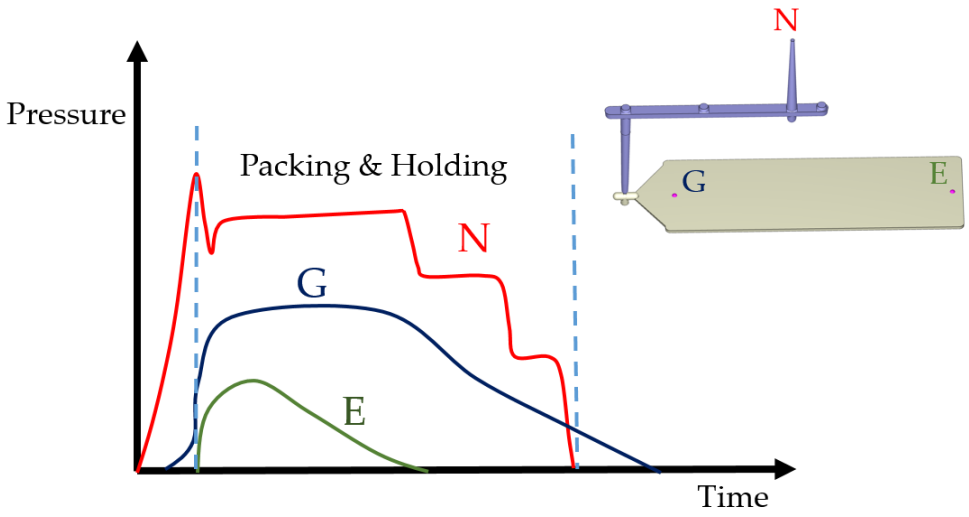

Figure 1.8 Typical pressure variations versus time at different locations

Schematic pressure variations versus position at filling and packing stages are shown in **Figure 1.9**. If the melt is incompressible, the pressure drop during the packing stage will be zero. If the melt is considered as slightly compressible fluid as a general understanding polymer, it will show a small pressure drop during packing. In the real world, the pressure drop is considerably higher than in the case of a slightly compressible fluid. So far, there is no good theorem to explain that, or no one has done a simulation incorporating a theoretical model to demonstrate how this occurs.

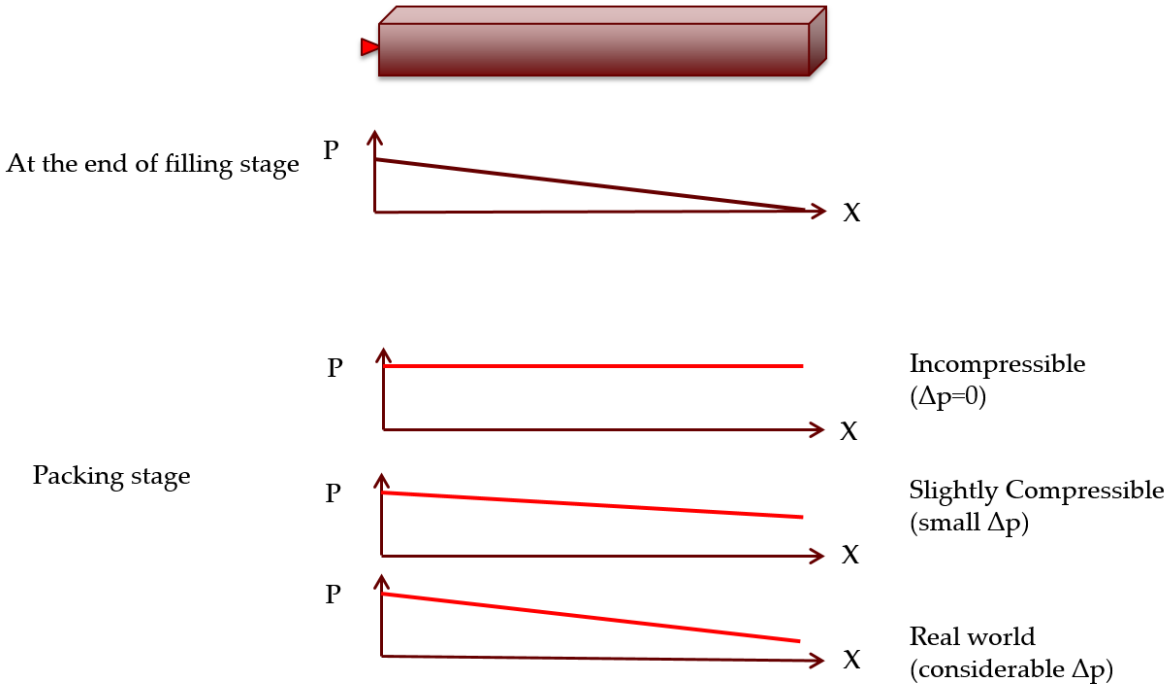

Figure 1.9 Schematic pressure variations versus position

Bulk viscoelasticity governs volume variation and density distribution in processing, and thus is expected to significantly influence injection molding in cavity pressures, shrinkage/warpage and thermally induced residual stress. However, bulk viscoelasticity is not well studied and understood in the field of polymer processing. The goal of this study is to demonstrate the influence of bulk viscoelasticity on injection molding, the research objectives of this dissertation are as follows:

Objective 1: Measuring and modeling of bulk viscoelasticity

a. Derive the bulk viscosity from PVT measurements
b. Develop a PVTQ model to describe the non-equilibrium PVT and assist in obtaining smooth and reliable bulk viscosity results
c. Find a model capable of describing the dependence of temperature, rate of volume change, and mechanical pressure on bulk viscosity

Objective 2: Simulating bulk viscoelasticity in injection molding

a. Predict the non-equilibrium PVT to verify the model and check if the fitting parameters are appropriate
b. Implement the bulk viscosity model into an injection molding simulation, and demonstrate the effects of bulk viscosity during packing stage

Objective 3: Validating and modifying constitutive models

a. Validate the bulk viscosity model with experimental cavity pressures
b. Propose corrections for the constitutive model to better fit the experimental cavity pressures
c. Use volumetric creep experiment data to determine model parameters and verify constitutive models
d. Validate the part weight and the shrinkage/warpage prediction with experimental result

2 Literature Review

Studies of bulk viscoelasticity are not as widely available in the literature when compared to shear viscoelasticity [4]. Bulk viscoelasticity can be observed by time-dependent bulk properties, such as bulk modulus, bulk compliance, volumetric coefficient of thermal expansion (CTE), and bulk viscosity. While bulk compliance/modulus is more intuitively adopted in solid mechanics formulation, bulk viscosity is commonly used in fluid mechanics formulation.

2.1 Time-dependent Bulk Compliance/Modulus

Time-dependent bulk compliance/modulus of polymeric materials, of which only a few experimental data are available, mainly were measured around the Tg [5-10] to make the volume change rate comparatively slow enough for observation. Various methods can be used [4-5], including sound absorption, transient volume creep experiment by applying a sudden pressure change (pressure jump) or sudden temperature change (temperature jump) [6-11], pressure relaxation experiment by applying a sudden volume jump [12-13], and volume measurement with dynamic/oscillating loading [14]. Those experimental data also help to explain physical aging, which means material properties (directly related to volume or indirectly affected by volume) evolve

with time and could be sensitive to past thermal and mechanical history [15]. Time-dependent bulk modulus master curves from pressure relaxation experiments performed by Meng et al. [13] show that properties can change by a factor of 2 to 3 for polymer melts (shown in **Figure 2.1**), while shear modulus can change by 3 orders of magnitude. Furthermore, the bulk modulus's relaxation spectrum differs from the shear modulus's.

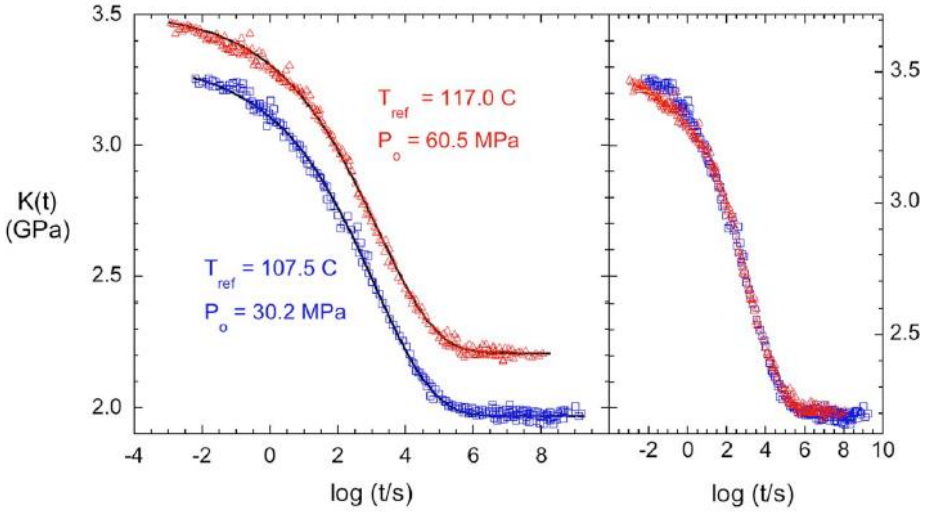

Figure 2.1 Time-dependent bulk modulus of polystyrene (Dylene 8 from Arco Polymers) [13]

2.2 Bulk Viscosity

There are two independent viscosities in isotropic Newtonian fluids (**Eq. 1.5**), the shear viscosity and bulk viscosity, respectively. While shear viscosity describes the resistance to changes of shape, bulk viscosity, also called volume

viscosity or dilatational viscosity, describes the irreversible resistance to the rate of volume change [16]. It is reasonable to neglect the bulk viscosity effect on flow field for monatomic gases and incompressible fluids. However, it is essential and not negligible for compressible fluids [16-19].

The studies of bulk viscosity using measurements, and its impact on flow fields have been growing in recent years, but most of the studies focus on gas or simple liquids [19-24]. There are only a few literature citations [25-28] that discuss the measurement and modeling of bulk viscosity of polymer melts. Bulk viscosity of polymer melts, especially how it varies across a wide temperature range, should be investigated in order to precisely evaluate the variation of density and volume during and after molding.

2.3 Measurement of Bulk Viscosity

Measuring bulk viscosity is more difficult than shear viscosity. However, it can be measured by sound attenuation involving potential experimental uncertainties [17], or by isothermal compression and expansion experiments. Lesbast, Legros, and Aleman [25] first attached a capillary rheometer to a tensile tester in order to measure the bulk viscosity of epoxide prepolymers under compression flow. They computed the bulk viscosity as pressure difference divided by compression rate, or change in volume deformation per unit time.

They found the bulk viscosity decreases with increasing compression rate, and that it could be 10^8 times larger than shear viscosity for epoxide prepolymers.

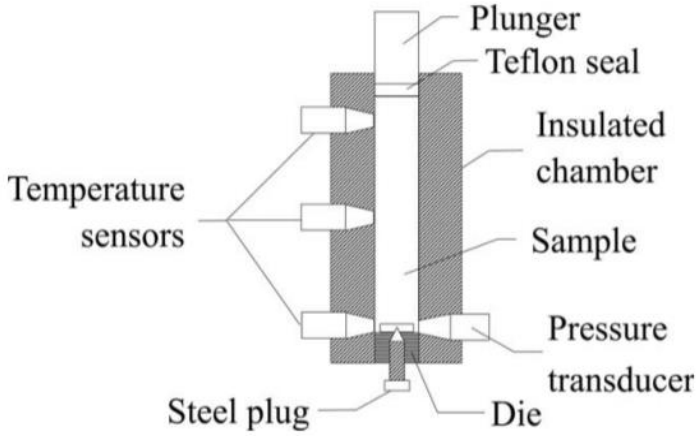

Figure 2.2 Schematic equipment of uniaxial compression experiment [28]

Aleman [26-27], and Chivapornthip and Bohez [28] adopted the same experimental setup, uniaxial compression (shown in **Figure 2.2**), to investigate the bulk viscosity of several polymer melts, such as polymethyl methacrylate (PMMA), isotactic polypropylene (iPP), polyvinyl chloride (PVC), polystyrene (PS) and low-density polyethylene (LDPE). They found that bulk viscosity, shown in **Figure 2.3**, in the melt state could be 10^4 times greater than the shear viscosity, and the range of magnitude typically could be around 10^4-10^5 MPa·s. Furthermore, they found that bulk viscosity decreases with increasing temperature and strain rate.

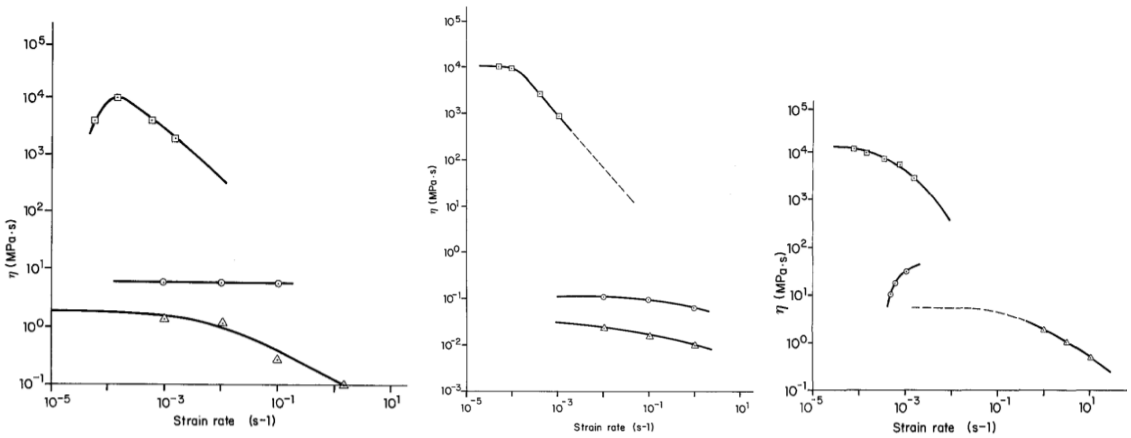

(a) PMMA at 438 K (b) i-PP at 453K (c) PVC at 453K

Figure 2.3 Bulk viscosity (□), elongational viscosity (○), and shear viscosity (△) of some polymer melts [26]

Shrinkage caused by cooling, or decrease in temperature, contributes a considerable amount of volume change, which cannot be measured using a uniaxial compression approach. It is also experimentally cumbersome to investigate the relationship of bulk viscosity to temperature by the uniaxial compression test. Therefore, cooling rate-controlled PVT (pressure-specific volume-temperature) measurements for bulk viscosity were developed in this study.

2.4 Modeling of Bulk Viscosity

Modeling the bulk viscosity, especially for polymer melts, is not well

developed yet. The Arrhenius equation has been used in the past to model the temperature dependence of bulk viscosity [25, 27], and higher order polynomials were use to describe the strain rate dependence [25, 28] (**Eq. 2.1** and **Eq. 2.2** respectively). However, the parameters of the empirical polynomials models do not have any physical meaning and do not represent the experimental data very well.

$$\begin{aligned} &\mu_d\left(T,\dot{\varepsilon}\right) = A_0 + A_1\left(\log a_T\dot{\varepsilon}\right) + A_2\left(\log a_T\dot{\varepsilon}\right)^2 + A_3\left(\log a_T\dot{\varepsilon}\right)^3 \\ &a_T = \exp\left[\frac{\Delta H_T}{R}\left(\frac{1}{T}-\frac{1}{T_0}\right)\right] \end{aligned} \tag{2.1}$$

$$\begin{aligned} &\log\mu_d = A_1\left(\log\Delta\dot{\varepsilon}\right) + A_2\left(\log\Delta\dot{\varepsilon}\right)^2 + A_3\Delta T^2 + A_4\left(\log\Delta\dot{\varepsilon}\right)\left(\log\Delta\varepsilon\right) \\ &+A_5\left(\log\Delta\dot{\varepsilon}\right)\Delta T + A_6\left(\log\Delta\varepsilon\right)\Delta T + A_7\left(\log\Delta\dot{\varepsilon}\right) + A_8\left(\log\Delta\varepsilon\right) + A_9\Delta T + \log\mu_0 \\ &\Delta\varepsilon = \varepsilon - \varepsilon_0 \\ &\Delta T = T - T_0 \end{aligned} \tag{2.2}$$

where A_i are data fitted coefficients; μ_0 is the bulk viscosity at zero strain ε_0, zero strain rate $\dot{\varepsilon}_0$ and the reference temperature T_0.

2.5 Bulk Viscoelasticity's Impact on Molding Processes

Chivapornthip and Bohez [28] were the first to recognize that the bulk viscosity could be a critical factor in influencing injection molding simulation, especially in the packing and holding stage. Since injection molding adopts high pressure to compress the material in order to overcome shrinkage caused by

cooling, the melt is compressed at high rates [29-30]. However, the influence of bulk viscosity on plastic molding is not clear, since bulk viscosity had not been included in the work of Chivapornthip et al. to test its influence.

Bulk viscoelasticity governs volume variation and density distribution in processing. It is expected to significantly influence injection molding in cavity pressures during the packing phase, shrinkage/warpage (dimensional changes in size and shape of injection-molded part), and thermally induced residual stress.

2.6 Simulation of Viscoelasticity

Several studies have dealt with the simulation of shrinkage/warpage or residual stress, but most did not consider bulk viscoelasticity [31-33]. Some studies consider time-dependent bulk modulus or time-dependent volumetric CTE by assuming those bulk properties share the same relaxation function as shear modulus [34-37]; however, this assumption may not be valid. Only a few studies consider bulk viscoelasticity to have a different relaxation spectrum than shear viscoelasticity [38-40]. To the best of our knowledge, all available simulations of shrinkage/warpage considering bulk viscoelasticity in literature over the years are computed by solid mechanics solvers, which means the flow effect on bulk deformation during molding may not be directly taken into

consideration.

Injection molding simulation has been maturely developed [30], and various numerical methods were continuously introduced into this field [41]. However, the simulation of bulk viscoelasticity in the packing stage is just starting to draw attention. Krebelj et al. [42] demonstrate a rate equation that models the cooling rate effect on specific volume and then simulates it in a fluid solver, but their simulation results show that the cooling rate effect almost made no difference on cavity pressure. In this study, constitutive models with bulk viscosity can represent specific volume cooling rate dependence and play a significant role in cavity pressure.

3 Experimental Setup

3.1 Material

General PS POLYREX® PG-33 from CHI MEI Corporation was used in this experiment. The characteristics of this material are listed in **Table** 3.1.

Table 3.1 Characteristics of General PS PG-33

Properties	Value
Supplier MFI (200°C)	8 [g/10 min]
Heat Distortion Temperature	87 [°C]
Density (23°C)	1.05 [g/cm^3]
Tensile Strength (Break)	460 [Kg/cm^2]
Flexural Strength	670 [Kg/cm^2]

3.2 Piston-type PVT Apparatus

A commercial piston-type GOTECH PVT-6000 apparatus, able to work according to ISO 17744:2004 and shown in **Figure 3.1**, is used to measure polymer melts' pressure-specific volume-temperature (PVT). The testing chamber, shaped as a cylinder with a diameter of 7.8 mm, contains the material, and a polytetrafluoroethylene (PTFE) seal (3.2 mm) is adopted to avoid leakage. Specific

volume is computed by measuring the longitudinal length of the testing chamber, where a heating/cooling system controls temperature and pressure is kept by applying monitored mechanical pressure on the piston.

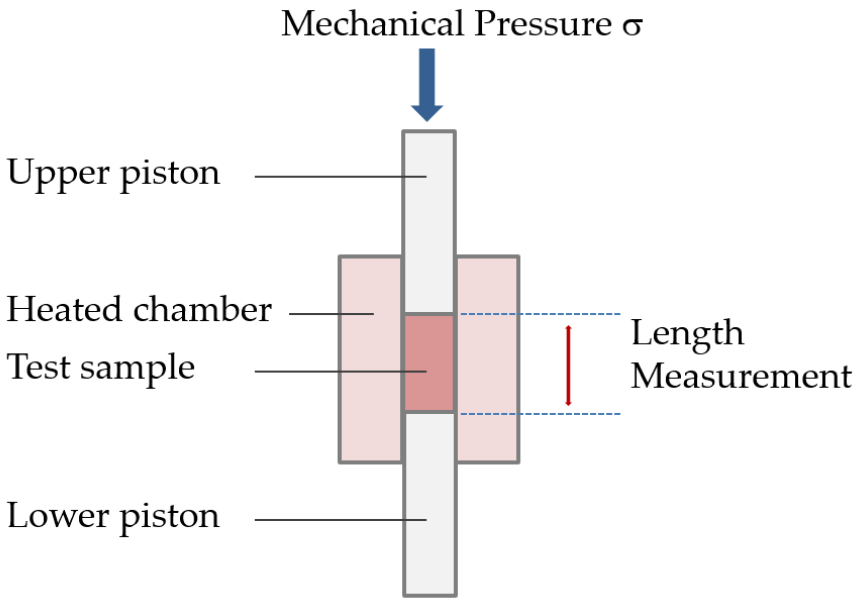

Figure 3.1 Piston-type PVT apparatus

The polymer pellets are first weighted, so the measured volume leads to an initial cylindrical longitudinal length of around 15mm. The pellets in the testing chamber are then melted at a set temperature and equilibrated for 5 mins. This commercial apparatus was designed for isobaric cooling, temperature scans by cooling down at fixed cooling rates, and mechanical pressures. The conditions in this study are listed in **Table 3.2**. A non-equilibrium PVT diagram of PS from isobaric cooling measurements is shown in **Figure 3.2**. Three cooling rates with

three mechanical pressures, constitute a total of nine PVT curves. Lower temperature or higher mechanical pressure reduces the free volume, leading to a lower specific volume. More discussions can be found in Section 4.2.

An isothermal pressurization (volumetric creep) experiment can be done by manual setting and self-data processing. The specific volume reduces as mechanical pressure increases from 300 to 900 bar, as shown in **Figure 3.3**. Both isobaric cooling and isothermal pressurization PVT measurements help comprehensively understand bulk viscoelasticity.

Table 3.2 Isobaric cooling conditions

Conditions	**Value**
Cooling rates (K/min)	0.1, 1, 10 [K/min]
Mechanical pressures	30, 90, 150 [MPa]

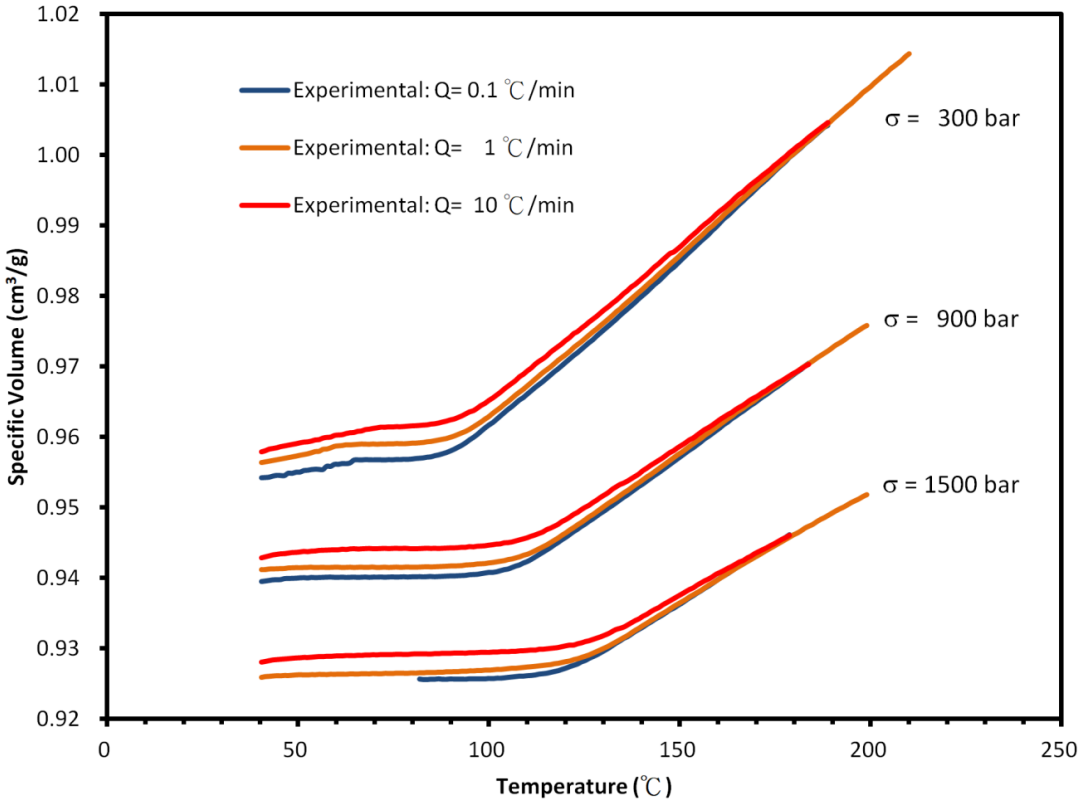

Figure 3.2 Isobaric cooling PVT of PS

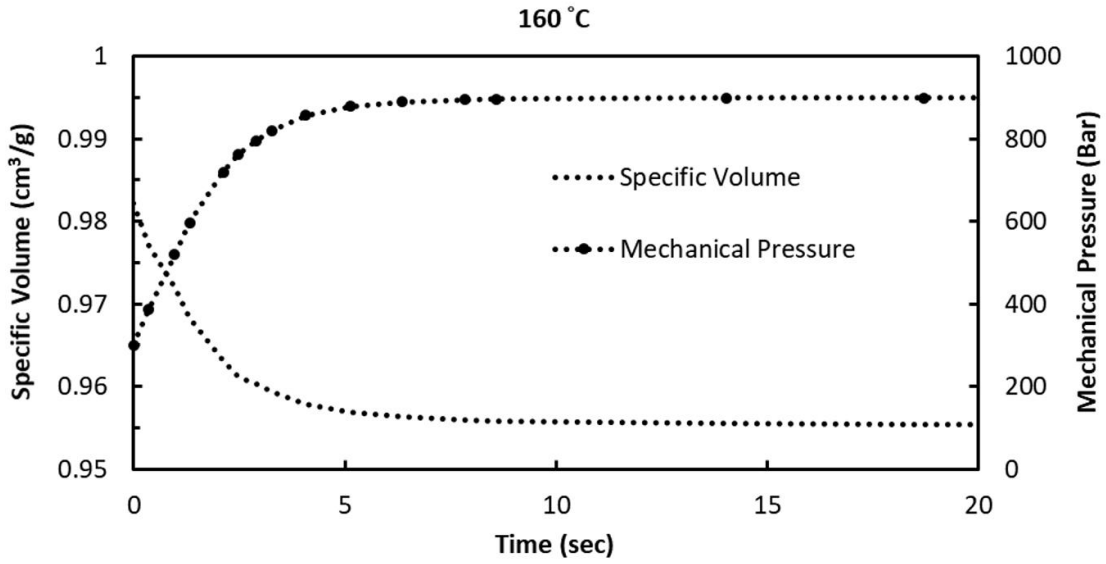

Figure 3.3 Volumetric creep experiment of PS at temperature 160 ℃

3.3 Injection Molding

A 3-plate mold (part size 300x 100x3 mm^3) with two Kistler pressure sensors (SN1 is close to the gate and SN2 is at the far end of the cavity) and an Arburg 630H-400 with screw diameter 40mm injection molding machine are used to record the cavity pressure variations during molding. A schematic of the injection molding cavity is shown in **Figure 3.4 (a)**.

The processing conditions used in injection molding are given in **Table 3.3**. During the filling stage, a uniform injection speed profile was used, resulting in an injection time of around 3.8 seconds. Three levels of packing profile were set for the packing and holding stage, starting with 800 bar for 10 seconds, then 400 bar for 0.5 seconds, and 200 bar for another 0.5 seconds. After molding, 5 ejected parts were weighted and measured in dimensions along length and width directions, as shown in **Figure 3.4 (b)**. Three lengths, L1, L2, and L3, were measured 25 mm above the center line, at the center line, and 25 mm below the center line, respectively. Three widths, W1, W2, and W3, were measured 75 mm, 150 mm, and 225 mm away from the gate, respectively. The following section compares cavity pressure variations, average weight, and average shrinkage with the model predictions to validate the simulation using bulk viscoelasticity.

Table 3.3 Molding conditions

Molding conditions	Value
Resin	General PS PG-33
Melt Temperature	197 [°C]
Mold Temperature	50 [°C]
Filling Time	3.8 [sec]
Packing Pressure Profile	800 [Bar] for 10 sec
	400 [Bar] for 0.5 sec
	200 [Bar] for 0.5 sec
Total Packing Time	11 [sec]
Cooling Time	50 [sec]

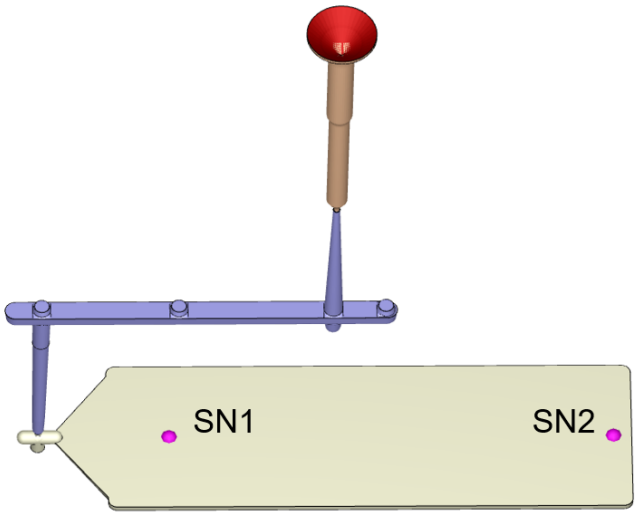

(a) Part geometry and sensor locations

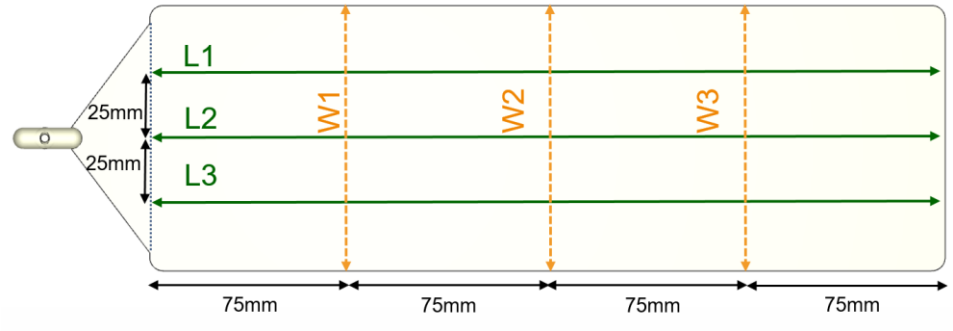

(b) Length and width measurement locations

Figure 3.4 Schematic of the injection molding cavity

The experimental pressure variations versus time at different locations are shown in **Figure 3.5**. During the filling stage, the nozzle pressure is increased to provide the driving force to inject the polymer melt into the cavity. After the Velocity/Pressure (VP) switch-over, the nozzle pressure dropped suddenly and then slowly increased to maintain a holding pressure. Comparing the nozzle pressure during packing to the packing pressure setting (constant 800 bar for 10 sec), the nozzle pressure is 8-10 MPa lower than the setting and changed gradually. This difference should be explored in the future, but is assumed not be caused by bulk viscoelasticity for now.

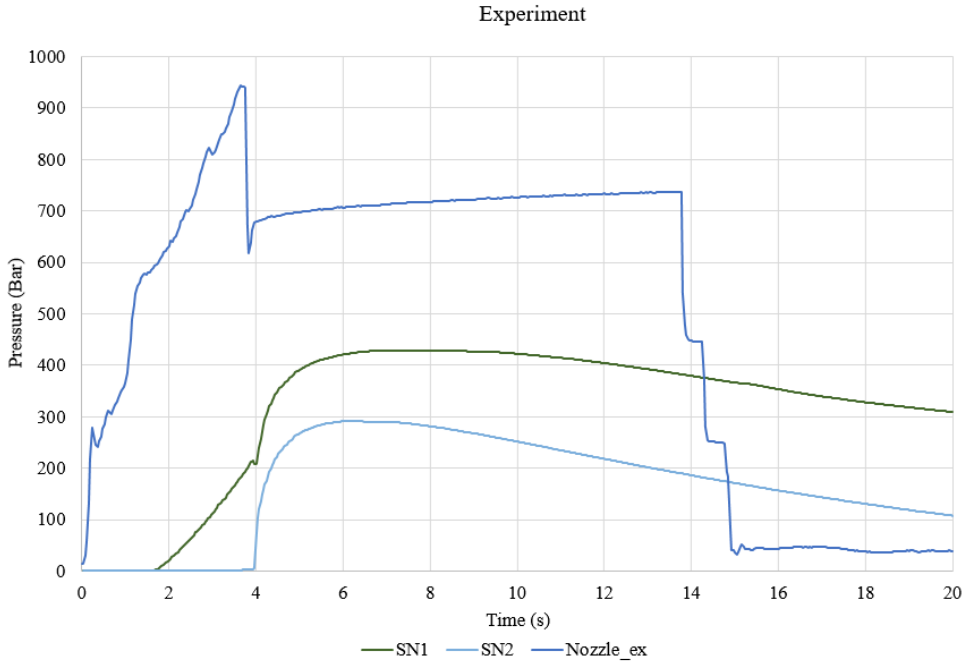

Figure 3.5 Pressure variations versus time at different locations

During the packing stage, experimental cavity pressure changed slowly and sustained a particular value until 20 seconds. In early packing, the pressure drops between nozzle and SN1, or between SN1 and SN2, remain considerably high. The high pressure drops during the packing stage are strongly related to a compressible fluid's volume change and are also correlated to bulk viscosity. The elongational viscosity, pressure-dependent shear viscosity and machine response of a hydraulic injection unit may play some roles in the pressure variations, but those are neglected for now in order to focus on the bulk viscoelasticity effect. Once bulk viscoelasticity effects are clarified, those effects can be further considered.

4 Measurement and Modeling of Bulk Viscosity in Generalized Newtonian Fluids

In this chapter, the full impact of bulk viscosity in Generalized Newtonian fluids is addressed, from measurement and model derivation, through modeling to the molding simulation. A cooling rate-controlled PVT (pressure-specific volume-temperature) measurement is implemented to measure the bulk viscosity over a wide temperature range. A new PVTQ (pressure-specific volume-temperature-cooling rate) model is then introduced to obtain better bulk viscosity data. Bulk viscosity was found to be well represented by a Cross-WLF(William-Landel-Ferry)-Arrhenius model. Finally, a molding simulation shows bulk viscosity significantly influences the cavity pressure in the packing and holding stage of the injection molding process.

4.1 Mechanical Pressure and Hydrostatic Pressure

Bulk viscosity is zero for ideal monatomic gases and the stress term containing bulk viscosity vanishes for incompressible fluids [44]. Hence, bulk viscosity was neglected in past decades although it may play an important role in dense fluids undergoing strong compression.

There are two definitions of pressure which must be further clarified. First is

hydrostatic pressure, or thermodynamic pressure, which is the exhibited pressure while the fluid is at rest and under thermodynamic equilibrium. Second is mechanical pressure, which is often used to describe the mean value of normal stress while the fluids are in motion. In this study, σ is used to represent the mechanical pressure. The relationship between the mechanical pressure and hydrostatic pressure can be derived from **Eq. 1.5**, and is given by:

$$\sigma = -\frac{1}{3}\left(\boldsymbol{\pi}_{xx} + \boldsymbol{\pi}_{yy} + \boldsymbol{\pi}_{zz}\right) = p - \mu_d\left(\nabla \cdot \mathbf{u}\right) \tag{4.1}$$

A similar idea and derivation can be found in [17,20].

4.2 Measurement of Non-equilibrium PVT

Non-equilibrium PVT diagrams of General PS POLYREX® PG-33 measured by piston type GOTECH PVT-6000 apparatus is shown in **Figure 4.1**. Three cooling rates with three mechanical pressures, bring a total of nine PVT curves. The specific volume of the polymer melt can be recognized as the volume occupied by molecular chains and the free volume between those molecular chains. Higher mechanical pressure reduces the free volume by forcing the molecular chains closer together, leading to a lower specific volume.

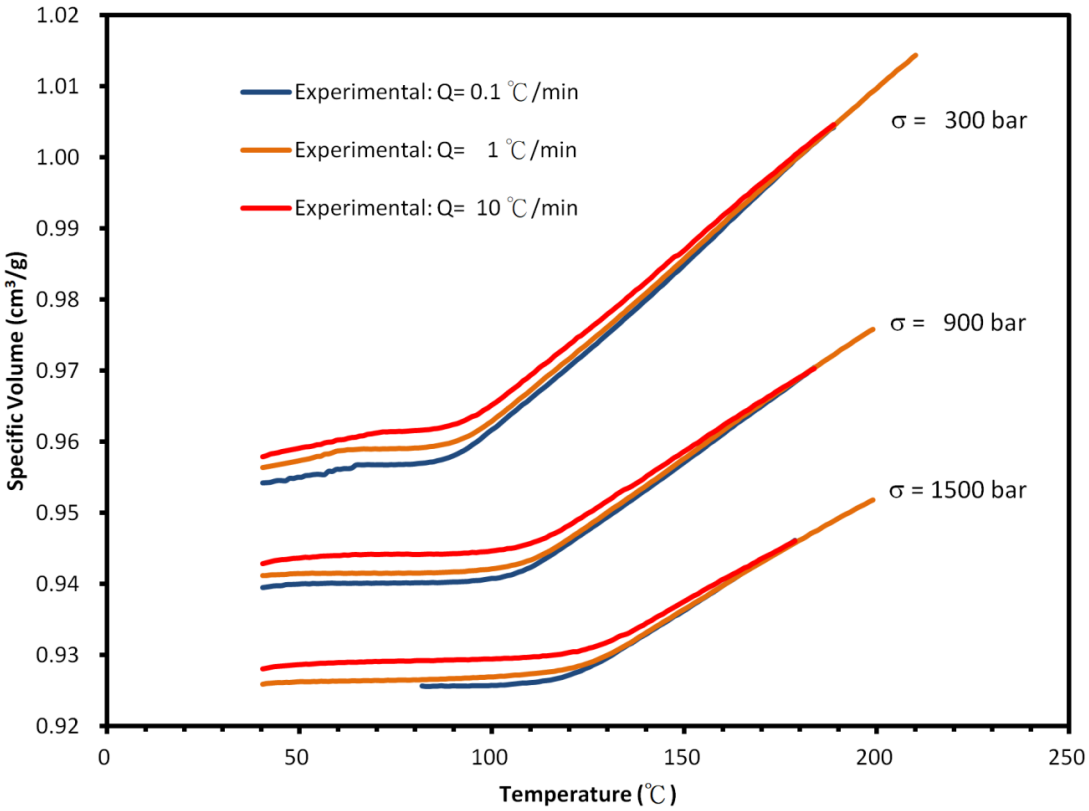

Figure 4.1 Non-equilibrium PVT diagram of PS

Cooling rate effect can be observed by comparing curves with a fixed mechanical pressure. A faster cooling rate is found to exhibit a higher specific volume, which is believed to be caused by a higher free volume, due to insufficient time to reach an equilibrium state. A faster cooling rate also shifts the transition temperature to a higher value. The same observations appear in references [42, 46].

A measured PVT diagram that follows ISO 17744:2004, with maximum permissible cooling rates is 5 °C/min, can be regarded as an equilibrium PVT under some circumstances or industrial application. However, **Figure 4.1** clearly shows that the PVT curve still changes significantly while using 0.1 ℃/min, which means

that a very slow cooling rate is required to get the equilibrium PVT. However, such an extremely slow cooling rate is unrealistic. The later introduced PVTQ model may help address this problem by adding the capability of extrapolating the equilibrium PVT.

4.3 Equilibrium Pressure and Bulk Viscosity

For thermoplastics polymers, the equation of state is in the form of $\hat{v} = \hat{v}(p,T)$, which is recognized as an equilibrium PVT which can be obtained by a measurement with an extremely slow cooling rate. The two-domain Tait equation [42, 45-47] is a commonly used model for describing equilibrium PVT.

However, if a higher cooling rate is applied, the PVT diagram will differ from the equilibrium state [42, 46], in this case it is a non-equilibrium PVT. For any specific volume data from a non-equilibrium PVT curve, there exists an equilibrium pressure at the same temperature, and this equilibrium pressure can be found using the following relationship:

$$\hat{v}(\sigma,T,Q)_{non-equilibrium\ \mathrm{PVT}} = \hat{v}(p,T)_{equilibrium\ \mathrm{PVT}} \tag{4.2}$$

where $\hat{v}$ is a specific volume; σ is a mechanical pressure; T is a temperature; Q is a cooling rate; p is the equilibrium pressure.

The difference between mechanical pressure and equilibrium pressure is due

to a resistance force to fluid motion, which is given by **Eq. 4.1**. Therefore, the bulk viscosity can be obtained based on the following expression:

$$\mu_d = \frac{p - \sigma}{\nabla \cdot \mathbf{u}} \tag{4.3}$$

where σ is a mechanical pressure on the material; p is a calculated equilibrium pressure; and $\nabla \cdot \mathbf{u}$ is the rate of volume change.

4.4 PVTQ Model

The equilibrium PVT Model is essential for the quality of derived bulk viscosity results. Although a two-domain Tait equation is commonly used to model the equilibrium PVT of polymers, it is not good enough in this application due to the sharp transition from the melt to the solid state for amorphous materials and the fact that it does not consider cooling rate effects [47].

In order to consider cooling rate effects and have more flexibility of controlling PVT characteristics of melt-transition-solid state, a three stage volumetric coefficient of thermal expansion PVTQ Model, schematically depicted in **Figure 4.2**, is proposed. This PVTQ model can be used to derive the rate of volume change, which is smoother than the results directly calculated from the experimental data.

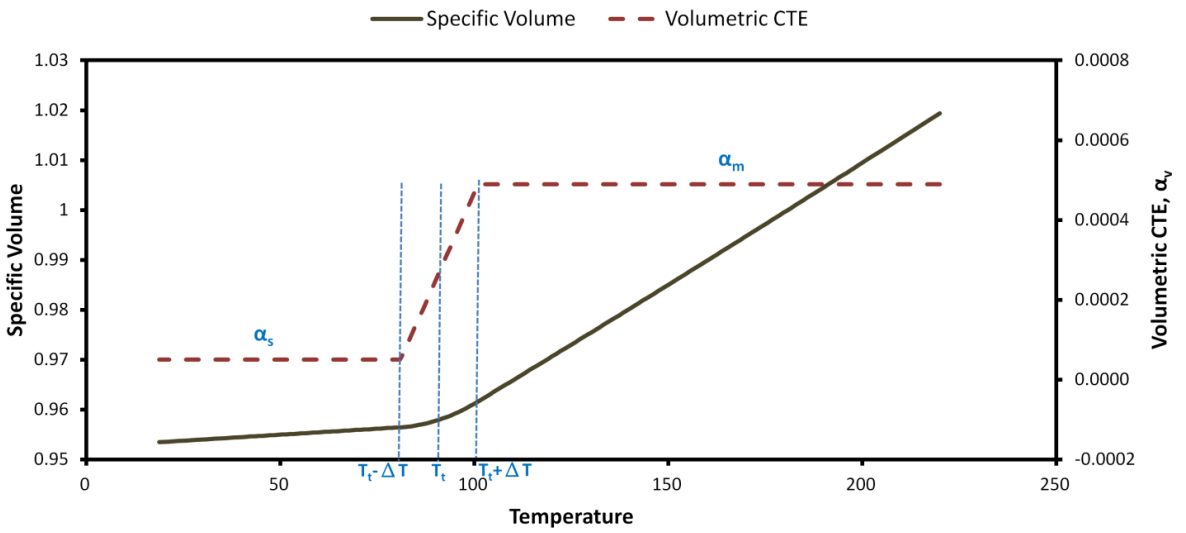

Figure 4.2 Illustration of three stages volumetric coefficient of thermal expansion

PVTQ Model

The specific volume is described as:

$$\hat{v} = \hat{v}_t \exp\left(\int_{T_t}^{T} \alpha_v dT\right) \tag{4.4}$$

Where $\hat{v}_t$ is the specific volume at the transition temperature; T is the temperature; T_t is the transition temperature; α_v is a volumetric CTE (volumetric coefficient of thermal expansion), which is a function of temperature T, pressure σ and cooling rate Q. This volumetric coefficient is divided into three stages according to melt-transition-solid state and is described as:

$$\alpha_v(T,\sigma,Q) = \begin{cases} \alpha_m, & \text{if } T \geq T_t+\Delta T \\ \alpha_s + \dfrac{\alpha_m - \alpha_s}{2\Delta T}\left(T - \left(T_t - \Delta T\right)\right), & \text{if } T_t-\Delta T<T< T_t+\Delta T \\ \alpha_s, & \text{if } T \leq T_t-\Delta T \end{cases} \tag{4.5}$$

where, α_m is the volumetric CTE in the molten state; α_s is the volumetric CTE in

the solid state; T_t is the transition temperature; ΔT is a control factor of the transition state. The above parameters and their relationships to temperature, mechanical pressure and cooling rate can be further described as follows:

$$
\begin{aligned}
T_t &= q_{T_t}\left(\ln(Q)-\ln(Q_{slow})\right)+(T_t)_{slow}\\
\alpha_m &= q_{\alpha_m}\left(\ln(Q)-\ln(Q_{slow})\right)+(\alpha_m)_{slow}\\
\alpha_s &= q_{\alpha_s}\left(\ln(Q)-\ln(Q_{slow})\right)+(\alpha_s)_{slow}\\
\hat{v}_t &= (\hat{v}_t)_{slow}\exp\left(\int_{T_t}^{T_m}(\alpha_m)_{slow}dT-\int_{T_t}^{T_m}\alpha_m dT\right)\\
(T_t)_{slow} &= a_{T_t}\sigma+b_{T_t}\\
(\alpha_m)_{slow} &= \alpha_{m1}+(\alpha_{m0}-\alpha_{m1})\left(1+(\lambda_m\sigma)^2\right)^{\frac{n_m-1}{2}}\\
(\alpha_s)_{slow} &= \alpha_{s1}+(\alpha_{s0}-\alpha_{s1})\left(1+(\lambda_s\sigma)^2\right)^{\frac{n_s-1}{2}}\\
(\hat{v}_t)_{slow} &= a_{\hat{v}_t}\sigma+b_{\hat{v}_t}
\end{aligned}
\tag{4.6}
$$

where Q_{slow} is the slowest cooling rate from the experiment; $\left(a_{T_t}, b_{T_t}\right)$ are the parameters to control pressure effect on transition temperature of the slowest cooling rate $(T_t)_{slow}$,which is assumed linearly depend on pressure; $\left(a_{\hat{v}_t}, b_{\hat{v}_t}\right)$ are the parameters to control pressure effect on specific volume at the transition temperature of the slowest cooling rate $(\hat{v}_t)_{slow}$, which is assumed linearly depend on pressure; $(\alpha_{m0}, \alpha_{m1}, \lambda_m, n_m)$ are the parameters to control pressure effect on volumetric CTE at the melt state of the slowest cooling rate $(\alpha_m)_{slow}$, which is assumed to behave like a Bird-Carreau model [48-49] with respect to pressure;

$(\alpha_{s0}, \alpha_{s1}, \lambda_s, n_s)$ are the parameters to control pressure effect on volumetric CTE at the solid state of the slowest cooling rate $(\alpha_s)_{slow}$, which is also assumed to behave like a Bird-Carreau model. Furthermore, cooling rate effects are assumed to linearly influence the transition temperature and volumetric CTE in a logarithmic scale [46-47]. q_{T_t} is the parameter to the control cooling rate effect on transition temperature, q_{α_m} is the parameter to control the cooling rate effect on volumetric CTE at the melt state, and q_{α_s} is the parameter to control the cooling rate effect on volumetric CTE at the solid state. T_H is an extremely high temperature that cooling rate effect can be neglected.

The proposed PVTQ Model can also be used to describe the equilibrium PVT as $\hat{v}(\sigma, T, Q_{eq})_{PVTQ}$, if a hypothetical equilibrium cooling rate Q_{eq} is used. Equilibrium cooling rate is defined as a cooling rate that is slow enough to give the material enough time to reach thermodynamic equilibrium state. Equilibrium cooling rate can be represented by the following expression:

$$Q_{eq} = NQ_{slow} \tag{4.7}$$

where N is a number substantially smaller than 1. If N is equal to 1, this means the slowest cooling rate from the experiment is adopted as the equilibrium cooling rate. If N is smaller than 1, this means the equilibrium PVT is extrapolated from experimental data by the proposed PVTQ model.

A non-equilibrium PVT is then fitted using a PVTQ model using the fitted parameters are listed in **Table 4.1**. The results of **Figure 4.3 (a)** demonstrate that the proposed PVTQ model is able to adequately describe non-equilibrium PVT of the general PS. Volumetric CTE can be obtained by the slope (first derivative) of the PVT curves, divided by the current volume, as shown in **Figure 4.3 (b)**. The CTE result is shown in logarithmic scale in order to display the variations. Starting and ending point of the phase transition can be clearly observed by the inflection points. The experimental inflection points are well matched by the model, suggesting the transition temperature T_t and the control factor ΔT are chosen well. Furthermore, while the experimental noises are obvious due to amplifications resulted from taking the first derivative of the measured PVT data, the curves generated using the PVTQ model are smooth. Consequently, a smooth rate of volume change and bulk viscosity, calculated using **Eq. 4.3**, are achieved.

Using this fitted PVTQ model, the PVT curve for cooling rates that are faster or slower than the ones available experimentally, can be extrapolated. The equilibrium PVT can then be extrapolated by assuming an equilibrium cooling rate, but the selection of an equilibrium cooling rate is essential. If the slowest cooling rate from the experiment is chosen, 0.1 ℃/min , zero bulk viscosity is obtained since there is no difference between mechanical pressure and equilibrium pressure. This

results in less useful experimental data of bulk viscosity and affects the fitting parameters in modeling. On the other hand, over extrapolation may introduce undesired errors if choosing a rate far lower than the slowest cooling rate (0.1 ℃/min). According to the experimentally available cooling rates (0.1, 1, 10 ℃/min), equilibrium cooling rate is assumed to be 0.01 ℃/min, and the parameter N of **Eq. 4.7** is set to 0.1.

Table 4.1 Fitted Parameters for PVTQ model

Parameters	Value
a_{T_t}	0.25 [°C /MPa]
b_{T_t}	83 [°C]
q_{T_t}	0.87 [°C /ln(°C/min)]
$a_{\hat{v}_t}$	-0.0002608 [1/MPa]
$b_{\hat{v}_t}$	0.9658 [-]
α_{m0}	5.5×10^{-4} [1/°C]
α_{m1}	3×10^{-4} [1/°C]
λ_m	0.03 [-]
n_m	0.01 [-]
q_{α_m}	-5×10^{-6} [1/ln(°C/min)]
α_{s0}	6.8×10^{-5} [1/°C]
α_{s1}	9×10^{-6} [1/°C]
λ_s	0.032 [-]
n_s	0.01 [-]
q_{α_s}	0 [1/ln(°C/min)]
T_H	220 [°C]

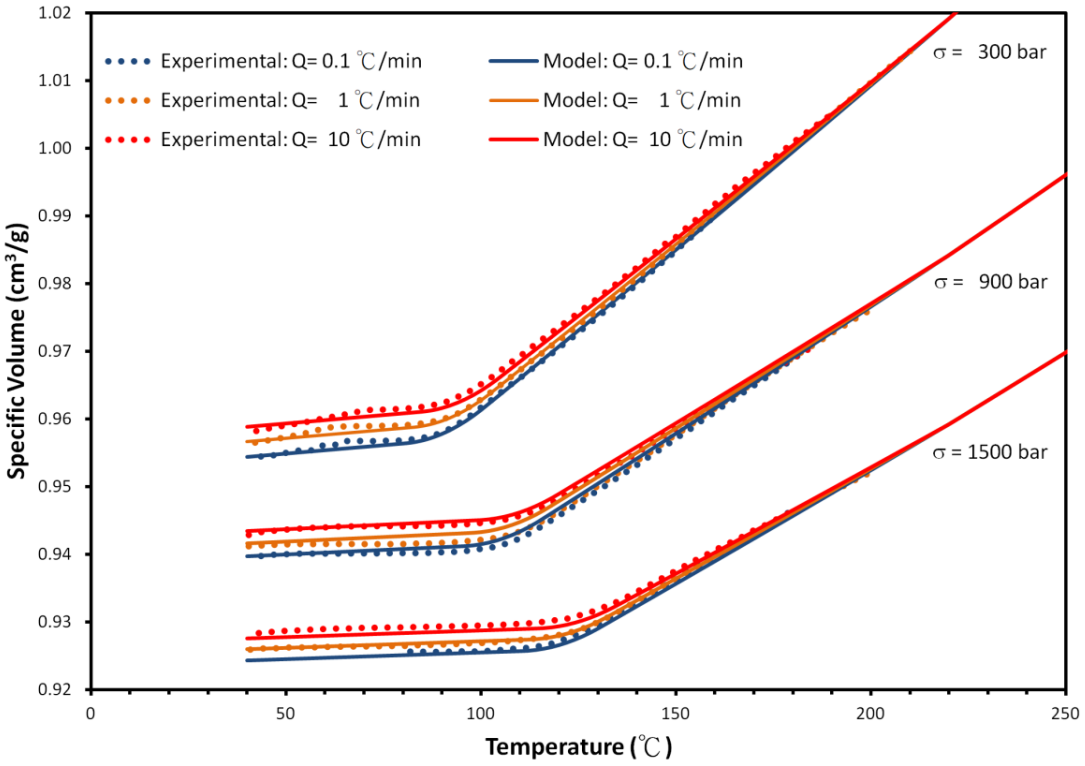

(a) Model described PVT diagram

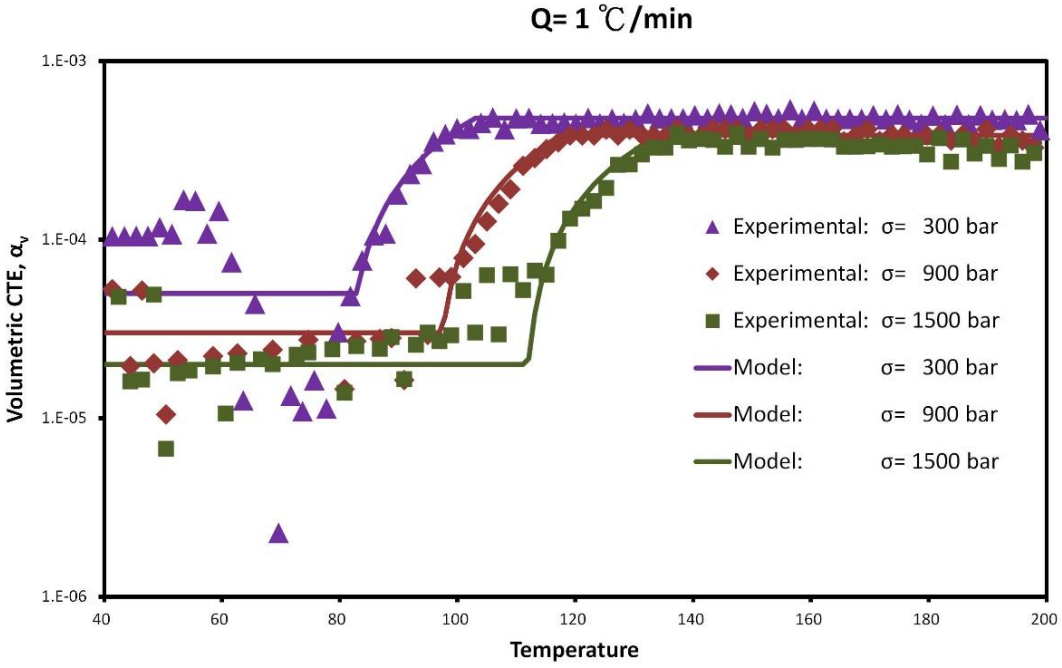

(b) Model described volumetric coefficient of thermal expansion

Figure 4.3 Comparison of PVTQ model and experimental data of PS

4.5 Bulk Viscosity versus Cooling Rate

Based on the fitted PVTQ model, any point on the non-equilibrium PVT curve of each cooling rate can find an equilibrium pressure that satisfies **Eq. 4.2**. The pressure difference between equilibrium pressure and mechanical pressure can be further used to derive the bulk viscosity. **Figure 4.4** shows bulk viscosity of this general PS for various cooling rates under a mechanical pressure of 300 bar. Three zones, melt zone, transition zone, and solid zone, can clearly be observed.

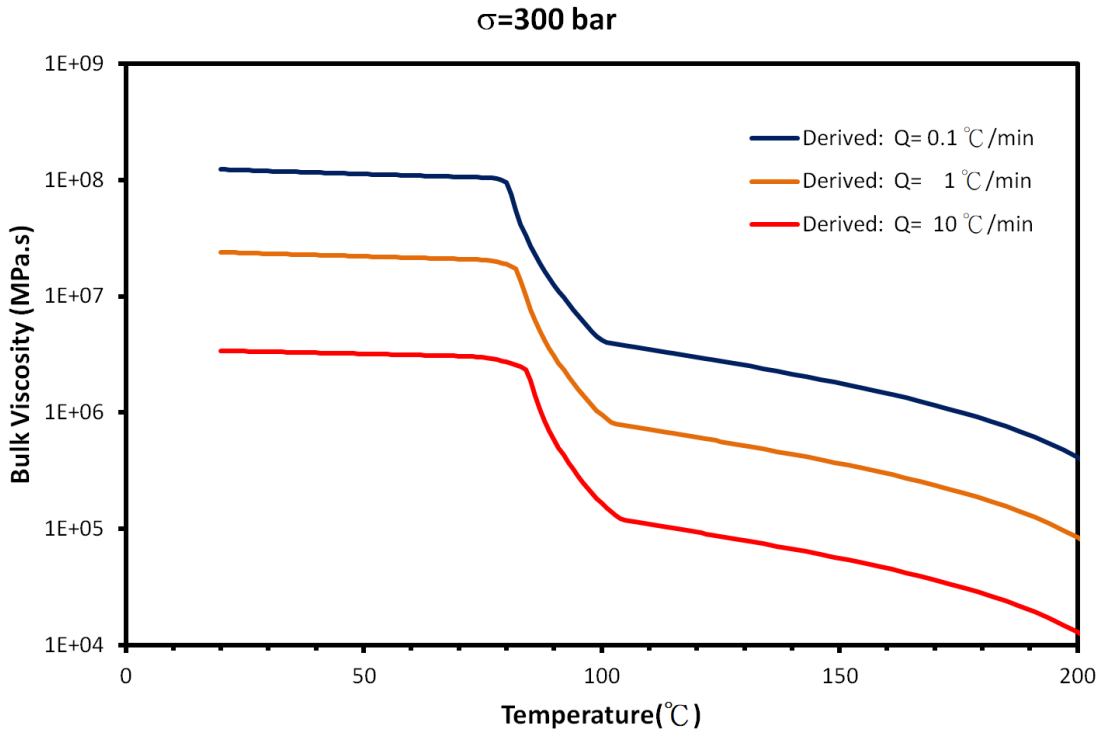

Figure 4.4 Bulk viscosity versus cooling rate of PS

In the melt zone, the mobility of molecular chains is high and the resistance to the volume change is low, which contributes to lower bulk viscosity. On the other hand, in the solid zone the mobility of molecular chains is low and the resistance to the volume change is high, which results to higher bulk viscosity. In the transition zone, the material exhibits a phase change from melt state to solid state, so bulk viscosity rises accordingly, and an abrupt change is observed. Moreover, bulk viscosity not only decreases with an increase of temperature but also decreases with the increase of cooling rate, or rate of volume change. The temperature range of transition, starting and ending point of transition, will be slightly different if changing from slower cooling rate to a faster cooling.

From a previous study by Aleman [26], the bulk viscosity of PS under the present condition of a fixed temperature (412 K), and fixed rates of volume change ranging from 5.4×10^{-5} to 13.5×10^{-5} s^{-1}, will lead to results ranging between 1×10^{4} and 4×10^{4} MPa·s. In this study, the bulk viscosity is 6.7×10^{4} MPa·s at the same temperature (412 K), cooling rate of 10 ℃/min and rate of volume change of 7.7×10^{-5} s^{-1}. These results are of the same order as in the previous study, showing that the current measurement technique and model are reasonable.

4.6 Bulk Viscosity versus Mechanical Pressure

Bulk viscosity versus mechanical pressure under a fixed cooling rate 0.1 ℃ /min is plotted as **Figure 4.5**. With increasing mechanical pressure, the distance between the polymer chains is reduced and the chain mobility is hindered. This lower mobility will lead to a higher bulk viscosity. At the same time increasing mechanical pressure shifts transition temperatures to a higher values.

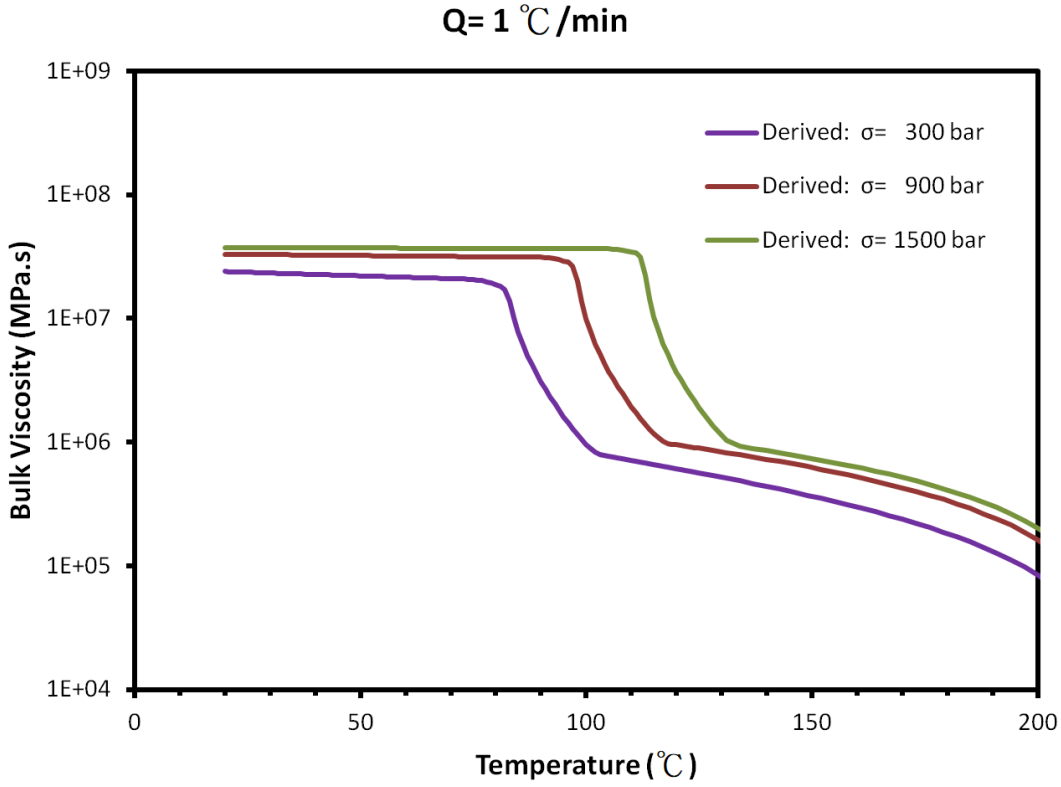

Figure 4.5 Bulk viscosity versus mechanical pressure of PS

4.7 Bulk Viscosity Modeling

The bulk viscosity of the polymer melt is represented as a Cross-WLF-Arrhenius like model, which has already been successfully used to describe the shear viscosity [50-52], viscoelasticity [53-54] and even for microbial inactivation [55]. A small modification is needed, so the strain rate is replaced by the magnitude of divergence $\nabla\cdot\mathbf{u}$, rate of volume change, using an expression:

$$\mu_d = \frac{\mu_0}{1+\left(\frac{\mu_0\left(\left|\nabla\cdot\mathbf{u}\right|\right)}{\tau^*}\right)^{1-n}}$$

$$\mu_0 = D_1 a^*$$

$$a^* = \begin{cases} \exp\left(\dfrac{-A_1\left(T-T^*\right)}{A_2+\left(T-T^*\right)}\right), \text{for T} \geq \text{T}^* \\ \exp\left(\dfrac{\Delta H_T}{R}\left(\dfrac{1}{T}-\dfrac{1}{T^*}\right)\right), \text{for T} < \text{T}^* \end{cases}$$

$$\begin{aligned} \text{T}^* &= D_2 + D_3\sigma \\ A_2 &= \tilde{A}_2 + D_3\sigma \end{aligned} \tag{4.8}$$

where T^* represents a solidifying temperature; μ_0 represents a bulk viscosity at a zero rate of volume change; τ^* represents a characteristic stress related to the volumetric stress at the transition between Newtonian and power-law behavior; n represents a power-law index; a^* represents a time–temperature shift factor including mechanical pressure effect. For temperatures below T^*, the Arrhenius model is used, using the activation energy, ΔH_T, and the gas constant, R. For

temperatures above T^*, the William-Landel-Ferry (WLF) model is used, using four experimentally determined parameters A_1, $\tilde{A}_2$, D_2 and D_3.

It is worthy to note that, there is a relationship between cooling rate and rate of volume, as $\nabla \cdot \mathbf{u} = \alpha_v Q$. So the effects of cooling rates Q can be substituted by the rates of volume change $\nabla \cdot \mathbf{u}$ by knowing the volumetric CTE α_v, which is almost a constant in the solid state and in the melt state. The dependencies of volumetric CTE to temperature, pressure and rate of volume change, can be covered in this Cross-WLF-Arrhenius-like model.

The experimentally derived bulk viscosity is then fitted by Cross-WLF-Arrhenius model, **Eq. 4.8**. The fitted parameters are listed as **Table 4.2**. Bulk viscosity described using the model has a reasonable agreement with experimentally derived data, as shown as **Figure 4.6** and **Figure 4.7**. This shows Cross-WLF-Arrhenius model is capable to represent the bulk viscosity as a function of temperature, pressure and cooling rate. In the modeling, cooling rate is replaced by rate of volume change.

Table 4.2 Fitted Parameters for Cross-WLF-Arrhenius Model

Parameters	Value
μ_0	4×10^{12} [MPa·s]
τ^*	0.7 [MPa]
n	0.2 [-]
$\Delta H_T / R$	2000 [K]
A_1	30 [-]
$\tilde{A}_2$	95 [K]
D_2	346.9 [K]
D_3	0.2416667 [K/MPa]

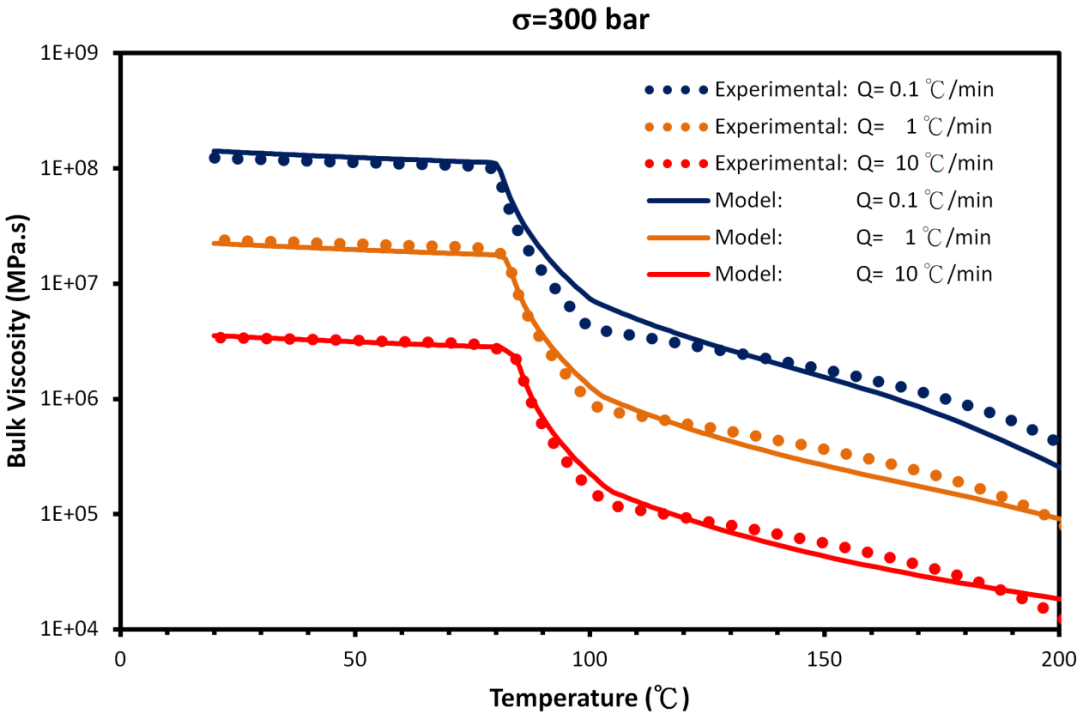

Figure 4.6 Model described bulk viscosity versus cooling rate of PS

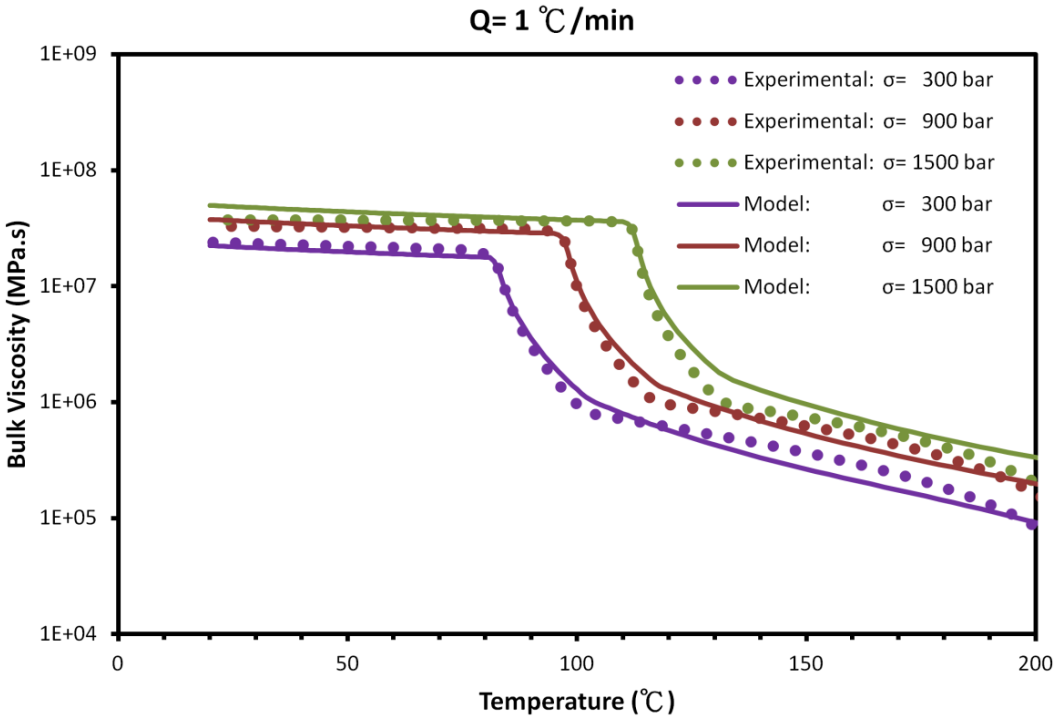

Figure 4.7 Model described bulk viscosity versus mechanical pressure of PS

4.8 Simulation for Solving Mechanical Pressure

The bulk viscosity effect is taken into consideration in the momentum equation, but its solution may be difficult to converge numerically. The general governing equations for 3D transient fluid flow are:

$$\rho\frac{\mathrm{D}\mathbf{u}}{\mathrm{D}t} = -\nabla p+\nabla\left(\left(\mu_d-\frac{2}{3}\eta\right)(\nabla\cdot\mathbf{u})\right)+\nabla\cdot\left(\eta\left(\nabla\mathbf{u}+\nabla\mathbf{u}^T\right)\right)$$

$$\nabla\cdot\rho\mathbf{u}=-\frac{\partial\rho}{\partial t} \qquad (4.9)$$

An approach to directly solve mechanical pressure σ instead of hydrostatic pressure p is proposed. The momentum equation is rewritten as:

$$\rho\frac{\mathrm{D}\mathbf{u}}{\mathrm{D}t} = -\nabla\sigma+\nabla\left(-\frac{2}{3}\eta\left(\nabla\cdot\mathbf{u}\right)\right)+\nabla\cdot\left(\eta\left(\nabla\mathbf{u}+\nabla\mathbf{u}^{T}\right)\right) \tag{4.10}$$

Mass conservation is further derived as followed:

$$\begin{aligned}\nabla\cdot\rho\mathbf{u} &= -\frac{\partial\rho}{\partial t}\\ &= -\left(\frac{\partial\rho}{\partial T}\right)_{p}\frac{\partial T}{\partial t}-\left(\frac{\partial\rho}{\partial p}\right)_{T}\frac{\partial p}{\partial t}\\ &= -\left(\frac{\partial\rho}{\partial T}\right)_{p}\frac{\partial T}{\partial t}-\left(\frac{\partial\rho}{\partial p}\right)_{T}\frac{\partial}{\partial t}\left(\sigma+\mu_{d}\left(\nabla\cdot\mathbf{u}\right)\right)\end{aligned} \tag{4.11}$$

More detail about considering of the dependence of the density on pressure and temperature in the mass conservation equation can be found in [56]. By the current proposed approach, the bulk viscosity effect has been moved from the momentum equation into the mass conservation equation through the equations rewritten above. This approach can help a common 3D transient fluid flow solver to more easily and stably take the bulk viscosity effect into consideration.

4.9 Non-equilibrium PVT Verification

Before a molding simulation is performed, a verification is made to ensure the fitted bulk viscosity and mass conservation (**Eq. 4.11**) can reproduce the non-equilibrium PVT curves. A computing cell is used to represent the PVT

measurement, which assumes the materials are homogeneous and uniformly distributed. This computing cell with an initial temperate 200℃ starts to cool down with various fixed cooling rates and under a fixed mechanical pressure 300 bar, as shown as **Figure 4.8**. The thermal expansion $\left(\frac{\partial \rho}{\partial T}\right)_p$ can be known by the equilibrium PVT, and thus rate of volume change can be obtained by solving the mass conservation. The specific volume at the next time step can be computed by the initial specific volume and rate of volume change. The predicted PVT curves are in agreement with experimental data, meaning the current modeling associated with bulk viscosity is able to describe the non-equilibrium PVT. Hence, this modeling approach is convincing and can be applied to a molding simulation with confidence.

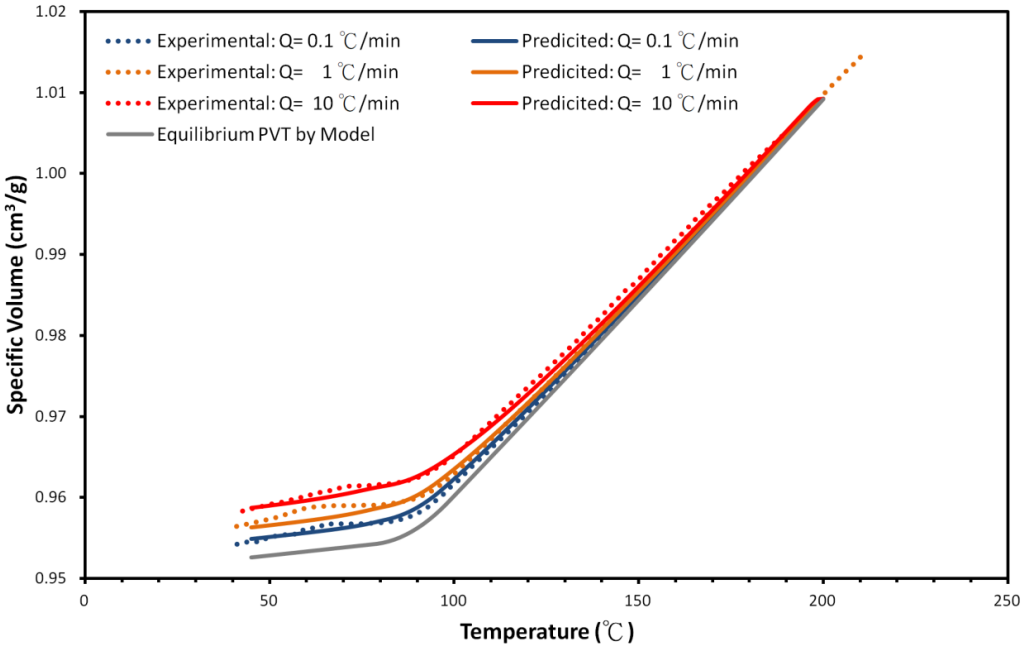

Figure 4.8 Non-equilibrium PVT curves predicted by this modeling

4.10 Molding Effect

Moldex3D, a commercial software with a finite volume method-based solver [57], was used to test the influence of bulk viscosity during a molding simulation. A tensile test bar, ASTM D638 Type I with a size 165x19x3.2 mm^3, is selected as a demo case. Two virtual sensors, SN1 and SN2, are added to demonstrate the bulk viscosity effect on cavity pressure in injection molding. The schematic of this test bar is shown in **Figure 4.9**. The molding condition is listed in **Table 4.3**.

Table 4.3 Molding condition of this demo case

Molding conditions	Value
Resins	General PS PG-33
Melt Temperature	190 [°C]
Mold Temperature	55 [°C]
Filling Time	0.5 [sec]
Packing Pressure	30 [MPa]
Packing Time	2 [sec]

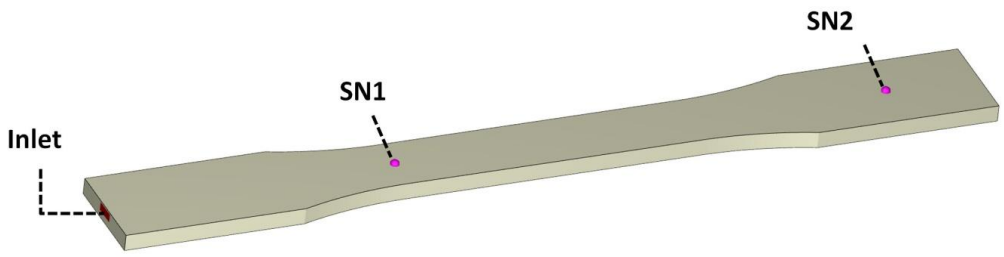

Figure 4.9 Schematic of ASTM tensile test bar

During the actual process, mechanical pressures are measured using pressure sensors and serve to control pressure at the inlet during the packing stage. Therefore, mechanical pressure distributions and variations are more critical than thermodynamic pressure. The mechanical pressure variation at the inlet, SN1 and SN2 are generated with (w/) and without (w/o) considering the bulk viscosity effect, as shown in **Figure 4.10**. During the filling stage, the mechanical pressure difference with and without considering bulk viscosity is negligible, since it is almost divergence free, or incompressible in the filling stage. However, in the packing stage, the material exhibits a significant volume change and shows the effect of compressibility. Therefore, the variation of mechanical pressure when considering the bulk viscosity effect is more minor, because bulk viscosity plays a role as a resistance preventing the molding resin from changing size, which also reduces pressure variations. Therefore, pressure builds up slowly in the early packing stage and decreases slowly in the following holding stage.

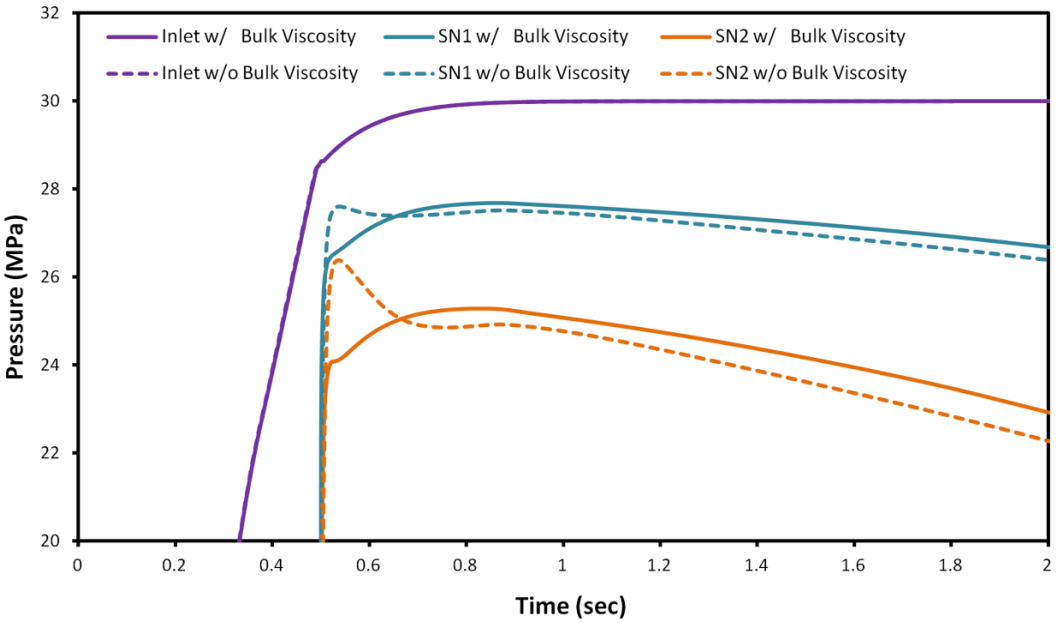

Figure 4.10 Mechanical pressure variations at the inlet, SN1 and SN2

The pressure drops between inlet and SN2 in the packing phase are plotted in **Figure 4.11**. The results demonstrate that the pressure drop with bulk viscosity effect changes slower than the case where effects of bulk viscosity effect are not included. The pressure drop variation is also significantly smaller for the simulation with bulk viscosity. Bulk viscosity prevents the material from changing its size quickly and contributes to maintaining the pressure drop from the inlet to the cavity. The effect of packing, significantly affects shrinkage and warpage, and will be quite different and inaccurate if bulk viscosity effects are not considered.

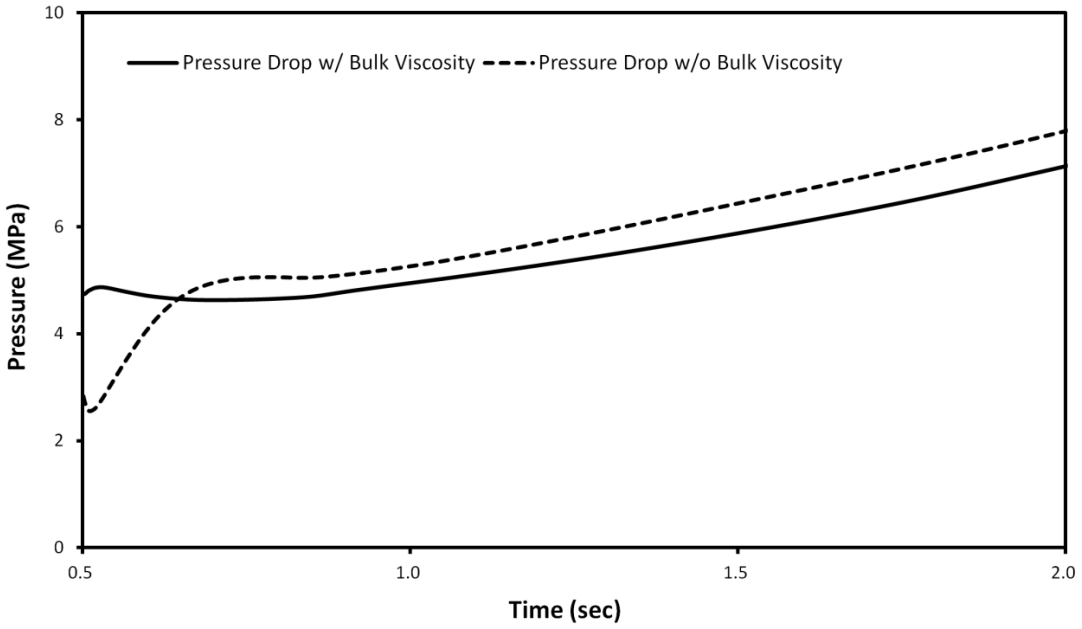

Figure 4.11 Pressure drops between inlet and SN2

5 Modeling and Simulation of Bulk Viscoelasticity in Injection Molding

The objective of this chapter is to simulate the bulk viscoelasticity based on a flow solver and show its influence on injection molding. Bulk viscoelasticity can be represented by the constitutive models with bulk viscosity and then considered for volumetric shrinkage through continuously computing variation of specific volume during filling, packing, cooling stage, and post-ejection. After ejection at every spatial point, volumetric shrinkages can be used as initial strain input for a linear elastic solid solver to solve for the dimensional changes of size and shape under static equilibrium.

A three-element-based model is proposed to better predict volume evolution than GNF (Generalized Newtonian Fluid) model. The proposed model significantly improves cavity pressure variations, part weights, and shrinkage predictions.

5.1 GNF Model (Kelvin-Voigt Model in Bulk Deformation)

As illustrated in **Figure 5.1 (a)**, the Newtonian fluid model can be analogized to a Kelvin-Voigt model, also revealed in citation [28], composed of a parallel

spring and dashpot. A Hookean spring describes the elastic effect that reversibly stores the strain energy and responds instantaneously to volumetric deformation. The Newtonian dashpot describes the bulk viscous effect related to the entropy caused by polymers' configurational rearrangement.

The spring force represents the equilibrium pressure p, and the spring constant is analogous to the bulk modulus K_e, which is the inverse of bulk compliance B_e derived from equilibrium PVT, also called isothermal compressibility. This Hookean spring could exhibit a volumetric CTE, α_e, derived from equilibrium PVT, which could also be regarded as a bulk compliance to thermal loading. We can write,

$$B_e = \frac{1}{\rho}\frac{\partial \rho}{\partial p} \tag{5.1}$$

$$\alpha_e = -\frac{1}{\rho}\frac{\partial \rho}{\partial T} \tag{5.2}$$

Where, ρ represents the density; Volumetric strain rate, $\dot{\varepsilon}_V$ (or $\nabla \cdot \mathbf{u}$), under any temperature change rate, $\dot{T}$, or pressure change rate, $\dot{p}$, can be written as:

$$\dot{\varepsilon}_V = \nabla \cdot \mathbf{u} = \alpha_e \dot{T} - B_e \dot{p} \tag{5.3}$$

Only the spring effect is considered for the GNF model without bulk viscosity, and the bulk deformation follows the equilibrium PVT. Any loading change will

instantaneously result in a volumetric strain and vice versa. It also immediately reaches thermodynamic equilibrium, at which point mechanical pressure equals equilibrium pressure. However, if bulk viscosity is present, the volumetric strain will be hindered by the dashpot, resulting in a difference between equilibrium and mechanical pressure.

Under a gradual loading change (creep experiment) from an initial mechanical pressure σ^0 to a new pressure σ^1 during a time increment Δt, the rate of volume change can be analytically derived as follows:

$$\nabla \cdot \mathbf{u} = -\frac{\left(\sigma^0 - p^0\right)}{\mu_d} e^{-t/\lambda} - B_e \frac{\sigma^1 - \sigma^0}{\Delta t}\left(1 - e^{-t/\lambda}\right) \tag{5.4}$$

where t represents the time; p^0 is the initial equilibrium pressure; $\lambda = B_e \mu_d$ is the retardation time, the characteristic time required for the spring to extend to its equilibrium length while retarded by the dashpot.

If the temperature effect is further taken into consideration, including a change from an initial temperature T^0 to a new temperature T^1, the equation can be obtained as follows:

$$\nabla \cdot \mathbf{u} = -\frac{\dot{\rho}}{\rho} = -\frac{\left(\sigma^0 - p^0\right)}{\mu_d} e^{-t/\lambda} - \frac{1}{\rho}\left(\left(\frac{\partial \rho}{\partial T}\right)_p \frac{(T^1 - T^0)}{\Delta t} + \left(\frac{\partial \rho}{\partial p}\right)_T \frac{\left(\sigma^1 - \sigma^0\right)}{\Delta t}\right)\left(1 - e^{-t/\lambda}\right) \tag{5.5}$$

Although the Kelvin-Voigt model (GNF model with nonzero bulk viscosity) can predict volume change slowly with a retardation effect, this model cannot describe the stress relaxation phenomena. It can also predict infinite stress under an instantaneous deformation, which is unrealistic for mechanics simulations.

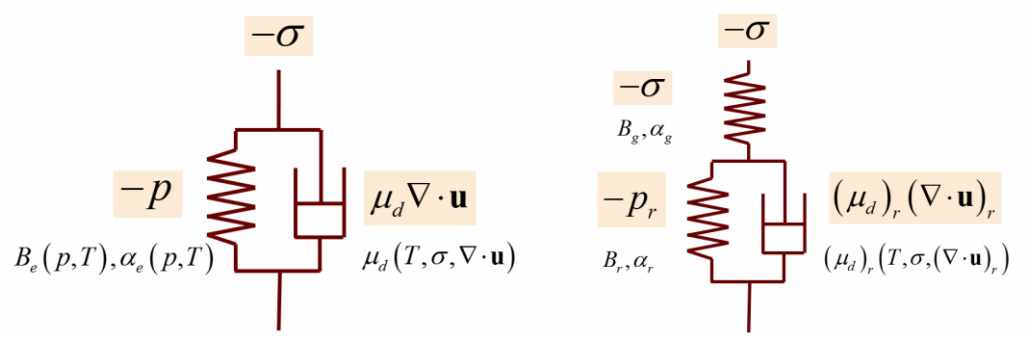

(a) (b)

Figure 5.1 Illustration of Generalized Newtonian Fluid Model (Kelvin–Voigt model) and proposed Three-element-based Model for bulk deformation

5.2 Three-element-based Model

A three-element-based model, or a kind of Standard Solid model, illustrated in **Figure 5.1 (b)**, is proposed in this paper since it can both reasonably predict creep and stress relaxation phenomena. The volume change rate is divided into rubber and glassy portions. The rubbery portion is considered by composing a

spring (rubbery spring) and dashpot (rubbery dashpot) in parallel, and the glassy portion is considered by adding a Hookean spring (glassy spring). The glassy spring could instantaneously result in bulk deformation under creep and help prevent infinite stress predictions in an instantaneous deformation but may be difficult to assess experimentally. The glassy spring and rubbery part (spring and dashpot in parallel) are designed to describe the bulk behavior of occupied volume (volume occupied by molecular chains) and free volume (free space between those molecular chains), respectively. Kovacs [58] first proposed similar ideas in 1961.

Under a gradual loading change, the rate of volume change for this three-element-based model is analytically derived as follows:

$$\nabla \cdot \mathbf{u} = -\frac{\dot{\rho}}{\rho} = -\frac{\left(\sigma^0 - {p_r}^0\right)}{\left(\mu_d\right)_r} e^{-t/\lambda_r} + \left(\frac{(T^1 - T^0)}{\Delta t}\right)\left(\alpha_r\left(1 - e^{\frac{-t}{\lambda_r}}\right) + \alpha_g\right) - \left(\frac{\left(\sigma^1 - \sigma^0\right)}{\Delta t}\right)\left(B_r\left(1 - e^{\frac{-t}{\lambda_r}}\right) + B_g\right) \tag{5.6}$$

where ${p_r}^0$ is the initial equilibrium pressure in the rubbery spring; $\left(\mu_d\right)_r$ is the bulk viscosity of the rubbery dashpot; $\lambda_r = B_r\left(\mu_d\right)_r$ is the retardation time in the rubbery portion; B_r is the bulk compliance of the rubbery spring; α_r is the volumetric CTE of the rubbery spring; B_g is the bulk compliance of the glassy

spring; α_g is the volumetric CTE of the glassy spring.

It is worth noting that the above models for bulk deformation, **Eq. 5.5** and **Eq. 5.6**, are objective since the volume change rate is a scalar [59], which can be obtained by the rate of density change, unlike shear viscoelasticity which requires transformations of strain tensor or rate of strain tensor to be frame-invariant under a change of frame with a spatial translation and a rotation.

The equilibrium pressure of this three-element-based model is desired to compute the density conveniently by equilibrium PVT, and it can be derived by **Eq. 5.3** as:

$$p = p_0 - \frac{\left(\nabla \cdot \mathbf{u} - \alpha_e \dot{T}\right)}{B_e} \Delta t \tag{5.7}$$

where p_0 is the equilibrium pressure at a previous time.

5.3 Deriving Bulk Viscosity of the Three-element-based Model

Since the three-element-based model is newly proposed, the approach to derive bulk viscosity from a cooling rate-controlled PVT measurement for the GNF model (Kelvin–Voigt model) needs to be revised. The equations and procedures are listed as follows:

$$\nabla \cdot \mathbf{u} = \left(\nabla \cdot \mathbf{u}\right)_r + \left(\nabla \cdot \mathbf{u}\right)_g \tag{5.8}$$

$$\left(\nabla\cdot\mathbf{u}\right)_g = \alpha_g \frac{T^1 - T^0}{\Delta t} - B_g \frac{\left(\sigma^1 - \sigma^0\right)}{\Delta t} \tag{5.9}$$

$$\left(\nabla\cdot\mathbf{u}\right)_r = \alpha_r \frac{T^1 - T^0}{\Delta t} - B_r \frac{\left(p_r - {p_r}^0\right)}{\Delta t} \tag{5.10}$$

$$\left(\mu_d\right)_r = \frac{p_r - \sigma}{\left(\nabla\cdot\mathbf{u}\right)_r} \tag{5.11}$$

Bulk compliances of the glassy spring (B_g and α_g) are suggested to be specified first, and the glassy portion of the volume change rate $\left(\nabla\cdot\mathbf{u}\right)_g$ can be known by **Eq. 5.9**. From known experimental volume change rates $\nabla\cdot\mathbf{u}$ and **Eq. 5.8**, the rubbery portion of the volume change rate $\left(\nabla\cdot\mathbf{u}\right)_r$ can be obtained. Next, bulk compliances of the rubbery spring (B_r and α_r) could be defined as functions of mechanical pressure, volumetric strain rate, or temperature. The current equilibrium pressure in the rubbery spring p_r can be determined based on **Eq. 5.10** and known initial conditions and cooling rate. Finally, the bulk viscosity of the rubbery dashpot $\left(\mu_d\right)_r$ in a three-element-based model can be derived by **Eq. 5.11**.

5.4 Chosen Bulk Compliances of Three-element-based Model

There could be many choices for designing the functions of bulk compliances for this three-element-based model. In this study, bulk compliances were designed to be determined by the available PVT data without requiring

additional experiments. It can be based on equilibrium PVT or the PVT measurement under the slowest available cooling rate. Furthermore, under the same mechanical pressure, the bulk compliances are chosen to be constants and not functions of temperature, meaning the temperature effect is only considered in bulk viscosity. However, the increasing bulk viscosity as the temperature is reduced retards the bulk deformation under load; thus, the equivalent (total) bulk compliance depends on temperature and time. The proposed bulk compliances and volumetric CTE are as follows:

$$\alpha_g = \left(\frac{1}{\rho} \frac{\partial \rho}{\partial T} \right)_{T_s}$$

$$\alpha_r + \alpha_g = \left(\frac{1}{\rho} \frac{\partial \rho}{\partial T} \right)_{T_H}$$

$$B_g = \left(\frac{1}{\rho} \frac{\partial \rho}{\partial p} \right)_{T_H} f$$

$$B_r + B_g = \left(\frac{1}{\rho} \frac{\partial \rho}{\partial p} \right)_{T_H} \tag{5.12}$$

where the volumetric CTE of the glassy spring α_g is assumed to be the same as the value in solid state (at a fixed temperature T_s); the summation of volumetric CTE is equal to the CTE value at an extremely high temperature T_H; the summation of bulk compliances are equal to the compressibility at an extremely high temperature T_H; bulk compliances of the glassy spring B_g is

assumed to be a ratio f times compressibility at an extremely high temperature T_H.

At an extremely high temperature T_H, the mobility of molecular chains is high enough to reach equilibrium rapidly during PVT measurements, so the equivalent (total) bulk compliances of this model should be kept the same as experimental values. However, the mobility of molecular chains is low in the solid state; cooling rate-controlled PVT measurements are believed to provide more accurate values in volume expansion coefficient than bulk compliance (compressibility). Hence, a ratio f is implemented to adjust reasonable glassy compressibility. The parameters used in this study are reasonably chosen based on the described behavior of polystyrene by PVTQ (pressure-specific volume-temperature-cooling rate) model and are listed in **Table 5.1**.

Table 5.1 Parameters related to bulk compliances

Parameters	Value
T_s	70 °C
T_H	220 [°C]
f	0.35 [-]

5.5 Predictions Using the GNF Model (Kelvin-Voigt Model in Bulk Deformation)

Predictions of bulk viscoelasticity can be known by computing the volume change (**Eq. 5.5** or **Eq. 5.6**) in a controlled cell with given initial conditions, material parameters, and loading changes (thermally or pressure-induced). From the previous chapter, the GNF model with (w/) bulk viscosity can predict isobaric cooling (cooling rate-controlled) PVT curves well. However, it cannot predict the newly introduced isothermal pressurization (bulk creep) data, shown in **Figure 5.2**.

For the case without (w/o) considering bulk viscosity, the specific volume changes with mechanical pressure without any perceivable delay. If bulk viscosity is considered, the specific volume changes slowly in the beginning and shows a noticeable delay in reaching a steady value of the specific volume. The experimental data undergoes a retardation effect when reaching a steady specific volume; however, it did not show a noticeable delay in the beginning, and most interestingly, the steady specific volume value is different from the one predicted by the GNF model without bulk viscosity (expected to be equilibrium PVT obtained by cooling rate-controlled measurements). A possible explanation is that the cooling rate used in the PVT measurements is still not slow enough for the

material to have enough time to reach equilibrium and therefore remains at a higher specific volume than the isothermal pressurization data.

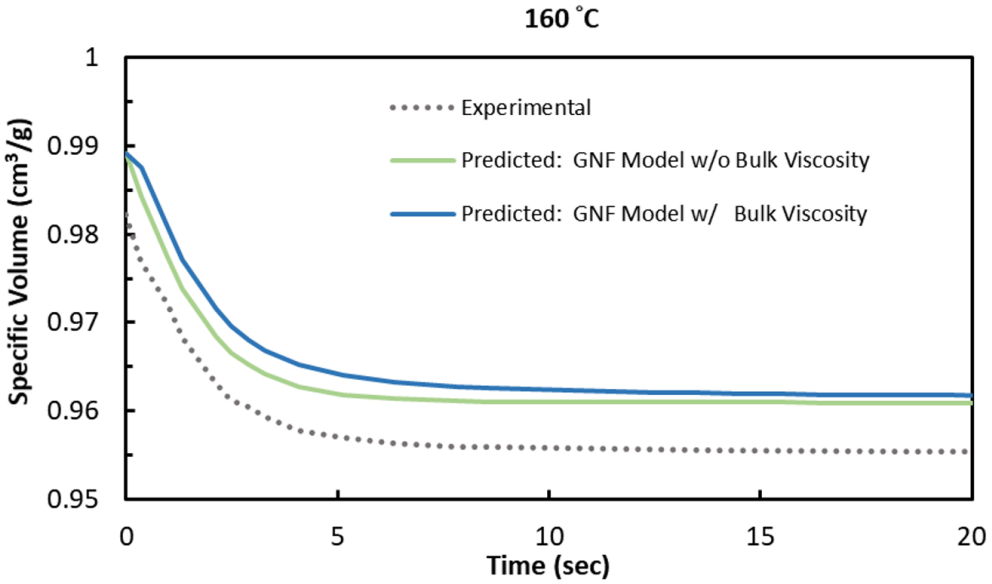

Figure 5.2 Bulk creep deformation predictions of Generalized Newtonian Fluid w/ and w/o considering the bulk viscosity at T=160 ℃

The simulated mechanical pressure variations using the GNF model and experimental data are shown in **Figure 5.3**. Many factors, such as material properties, numerical methods, mesh resolution, and machine response, could affect pressure predictions. Those factors may not be possible to address in this paper fully. In order to easily compare with experimental data, primarily focusing on the packing stage, the packing stage starts when the simulated inlet pressure reaches 943 bar, and the packing pressure profile in the simulation is set to follow

the experimentally recorded nozzle pressures. Thus, predicted pressure drops inside the cavity between different models can be easily compared based on the same inlet pressure variations.

As expected, mechanical pressure predictions are similar in the filling stage since it is almost divergence-free or incompressible during filling. On the other hand, predictions could be different in the packing stage since the material exhibits a significant volume change and shows the effect of compressibility. Without considering bulk viscosity, the simulated cavity pressure changed sharply at the beginning of the packing stage. When bulk viscosity was considered, the simulated cavity pressure changed somewhat smoother. However, the cavity pressures did not exhibit considerable differences between the GNF model, with and without considering bulk viscosity. Furthermore, while experimental cavity pressure decreased slowly and sustained a particular value until 20 seconds, both simulations predicted that cavity pressure decreased too fast over time.

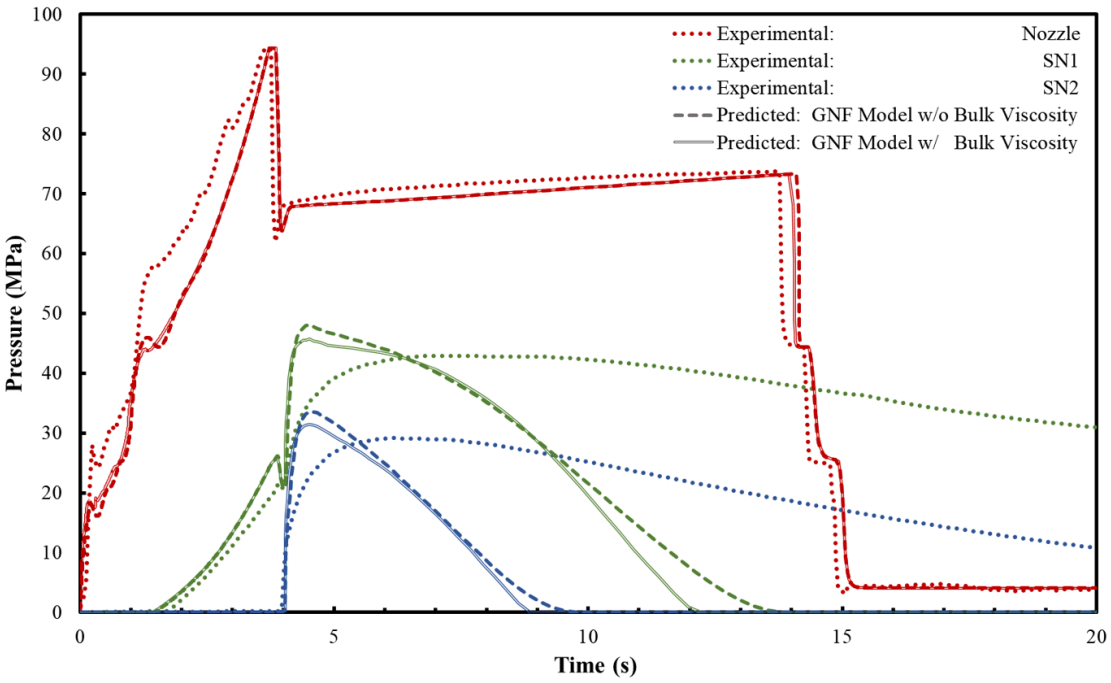

Figure 5.3 Mechanical pressure predictions for Generalized Newtonian Fluid w/ and w/o considering the bulk viscosity at the inlet, SN1, and SN2

5.6 Determination of Bulk Viscosity in Three-element-based Model

The disagreements between simulations using the GNF model and experiments, either from the bulk creep experiment or injection molding experiment, support the necessity of another bulk viscoelastic model, a three-element-based model, to improve the prediction for this amorphous polymer. The bulk viscosity of the three-element-based model $(\mu_d)_r$, including experimentally derived by **Eq. 5.8 - Eq. 5.11** from a cooling rate-controlled PVT measurement and described by the Cross-WLF-Arrhenius model (**Eq. 4.8**), is shown in **Figure 5.4**. The fitted parameters are listed in **Table 5.2**.

Table 5.2 Fitted Parameters for Cross-WLF-Arrhenius Model

Parameters	Value
μ_0	2.02E+12 (MPa·s)
τ^*	0.7 (MPa)
n	0.2 (-)
$\Delta H_T / R$	300000 (K)
A_1	25 (-)
$\tilde{A}_2$	95 (K)
D_2	350 (K)
D_3	0.2416667 (K/MPa)

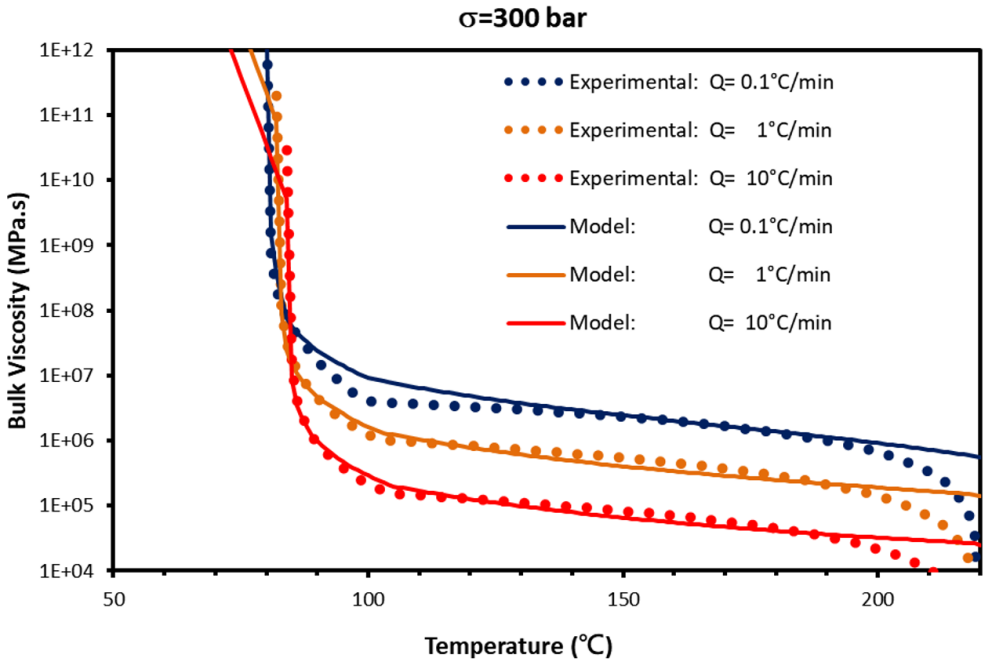

(a) Model described bulk viscosity versus cooling rate

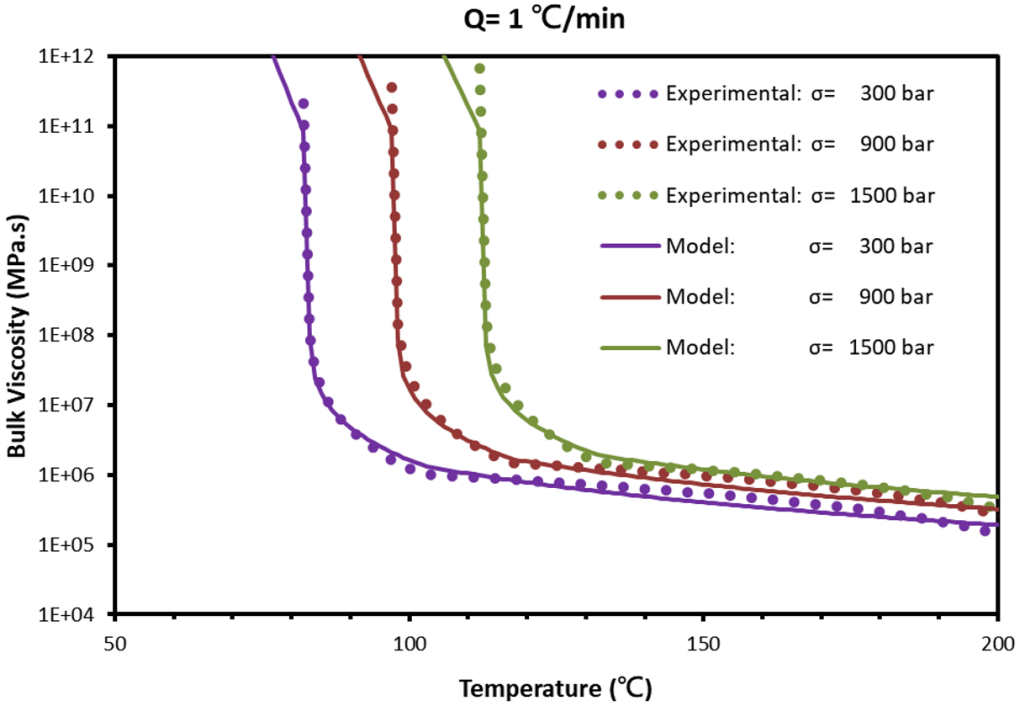

(b) Model described bulk viscosity versus mechanical pressure

Figure 5.4 Comparison of model and experimentally derived data of PS

As shown in **Figure 5.4 (a)**, the bulk viscosity is low in the melt state due to the high mobility of molecular chains. Bulk viscosity increases as the temperature is reduced and rises abruptly during phase transition. Experimentally derived bulk viscosity could reach an infinite value in the solid state because the volumetric CTE of the glassy spring (**Eq. 5.12**) is chosen to be the same as the value in the solid state, thus resulting in almost no rubbery portion of volume change rate. This helps simplify the problem that this amorphous polymer melt only exhibits an elastic effect in the solid state. However, this parameter can be chosen differently if desired.

At the extremely high temperature of about 220 ℃, experimentally derived bulk viscosity approaches zero since it is assumed that specific volumes under different cooling rates are the same, and bulk viscosity effect is negligible at such a high temperatures. Although this assumption is helpful when deriving the experimental bulk viscosity, the actual viscosity is not zero. However, it is not necessary for the model to approach zero at high temperatures due to the fact that useful processing range is below 200 ℃, a range at which the model renders accurate results.

Bulk viscosity vs. mechanical pressure under a fixed cooling rate of 0.1 ℃/min is shown in **Figure 5.4 (b)**. With increasing mechanical pressure, chain mobility is

hindered due to the reduced distance between the polymer chains, resulting in a higher bulk viscosity. The temperature, pressure, and volume change rate dependent Cross-WLF-Arrhenius model can reasonably describe the experimentally derived bulk viscosity, as shown in **Figure 5.4 (a)** and **5.4 (b)**.

Non-equilibrium PVT curves by cooling rate-controlled measurements under a fixed mechanical pressure of 300 bar can be predicted by the proposed three-element-based model with current fitting parameters, shown in **Figure 5.5**. In addition to cooling rate-controlled PVT curves, bulk creep deformation at a temperature of 160 ℃ can be well predicted by a three-element-based model, as shown in **Figure 5.6**. Both initial and final (steady) specific volumes in bulk creep deformation predicted by the three-element model are lower than those predicted by the GNF model, and it is closer to the experiment. This is because total bulk compliance by glassy and rubbery spring (B_g and B_r) could be higher than bulk compliance B_e at a temperature of 160 ℃. These verifications ensure that this modeling approach is convincing and can be confidently applied to a molding simulation.

It is worth noting that the model can predict the change of specific volume under hundreds of degrees per minute, which materials may exhibit during the injection molding. The predictions under the ultra-high cooling rates can be

regarded as extrapolations since the maximum cooling rate in PVT measurement is limited to 10 ℃/min because the temperature of materials inside the testing chamber cannot be assured uniform under the ultra-high cooling rates. The unavoidable extrapolations could reduce the accuracy of molding simulation but are believed to give reliable tendencies.

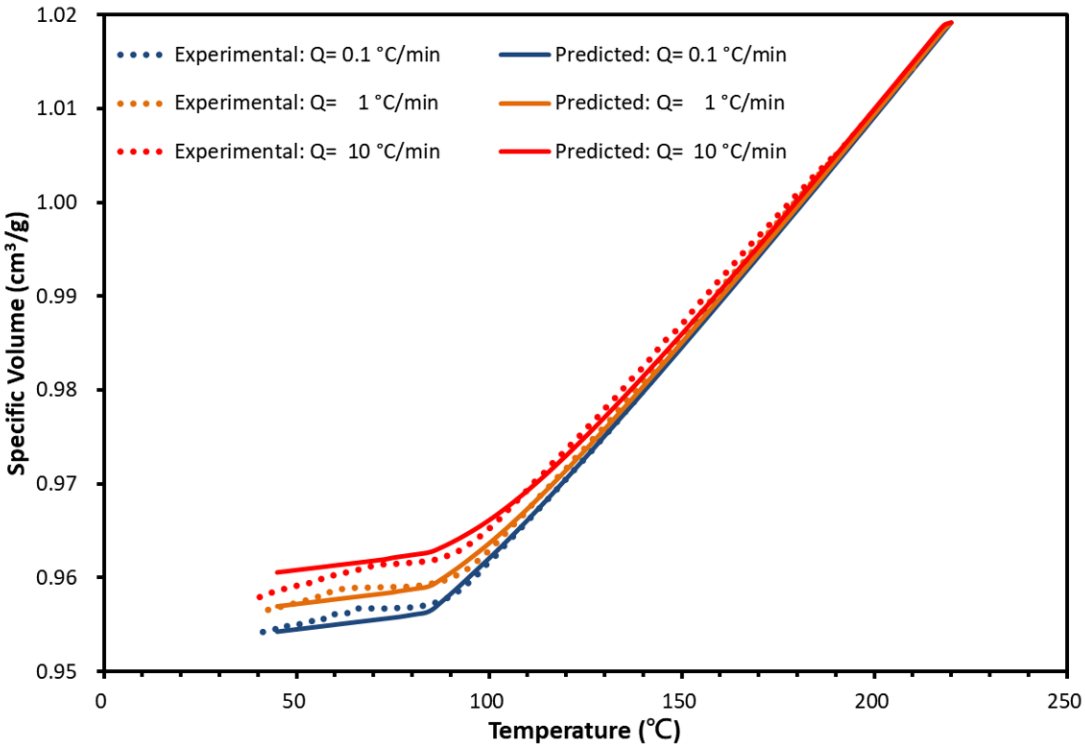

Figure 5.5 Isobaric cooling PVT curves predicted by this proposed three-element-based model

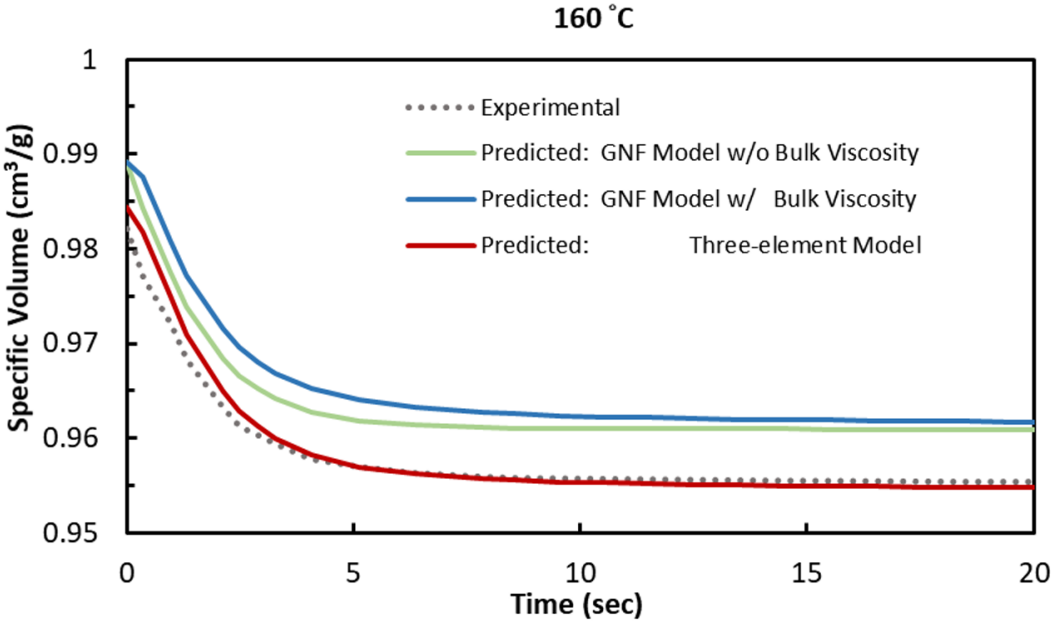

Figure 5.6 Bulk creep deformation predictions of the proposed three-element-based model at T=160 ℃

5.7 Predictions Using the Three-element-based Model

The simulated mechanical pressure variations by the three-element model and experimental data are shown in **Figure 5.7**. Predictions of mechanical pressure between the GNF and the three-element model during the filling stage are very close. While the GNF model without considering bulk viscosity predicts cavity pressures changing sharply in early packing and decreasing too fast over time, the three-element model can predict slower changes in cavity pressures and maintain higher values longer during packing. The model significantly improves

the predictions, although there is still a discrepancy between the simulation and experiment. This discrepancy may come from factors not considered in this study, like shear viscoelasticity. This discrepancy could be reduced by further studying bulk viscoelasticity.

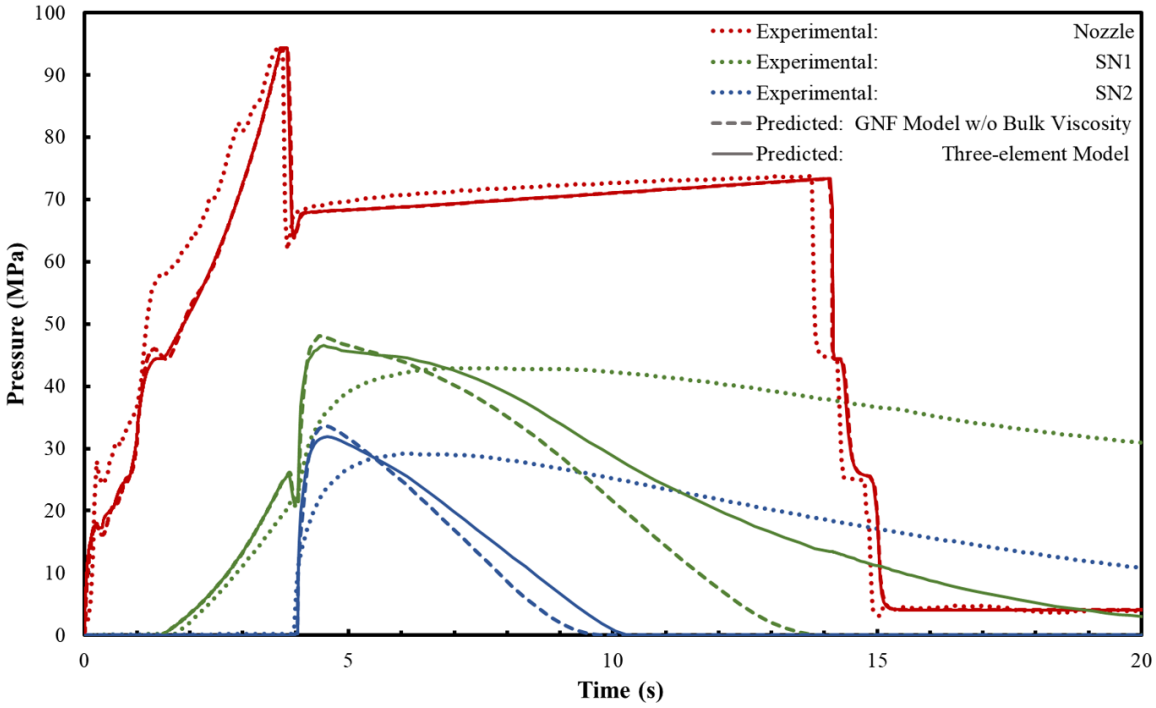

Figure 5.7 Mechanical pressure predictions for this proposed three-element-based model at inlet, SN1, and SN2

5.8 Volume Evolutions with Time on the PVT Diagram

Bulk viscoelasticity described by the GNF and the three-element-based model could influence the evaluation of specific volume with respect to the temperature and mechanical pressure changes during molding. A plot, **Figure 5.8**, was made on the PVT diagram to show the difference between three predictions of volume evolutions based on the same thermal and mechanical history during molding. This history was assumed to have an isothermal injection at first, where mechanical pressure rose from zero to 400 bar and temperature was kept at 200 ℃ for 2 seconds. This was followed by isobaric cooling during the packing stage, where the temperature was cooled to 160 ℃ and mechanical pressure was kept at 400 bar for 3 seconds. For the next 10 seconds during the cooling stage, the temperature was continually cooled to 130 ℃, and mechanical pressure was reduced to 50 bar. After the part was ejected, mechanical pressure was released to zero, and the temperature cooled down to room temperature with an assumed cooling rate of 60 ℃/min. The above history may not be wholly realistic but is adopted to show that the various models differently predict specific volumes. The volumetric shrinkage (shown below)

$$S_v = \frac{\hat{v}_c - \hat{v}_r}{\hat{v}_c}$$

is defined as the difference between the specific volume before ejection (at the end

of cooling), $\hat{v}_c$, and the specific volume at room temperature under atmospheric pressure, $\hat{v}_r$. **Table 5.3** shows that a single cell experiencing the same thermal and mechanical history predicted different volumetric shrinkages, and the three-element model predicted the most minor shrinkage.

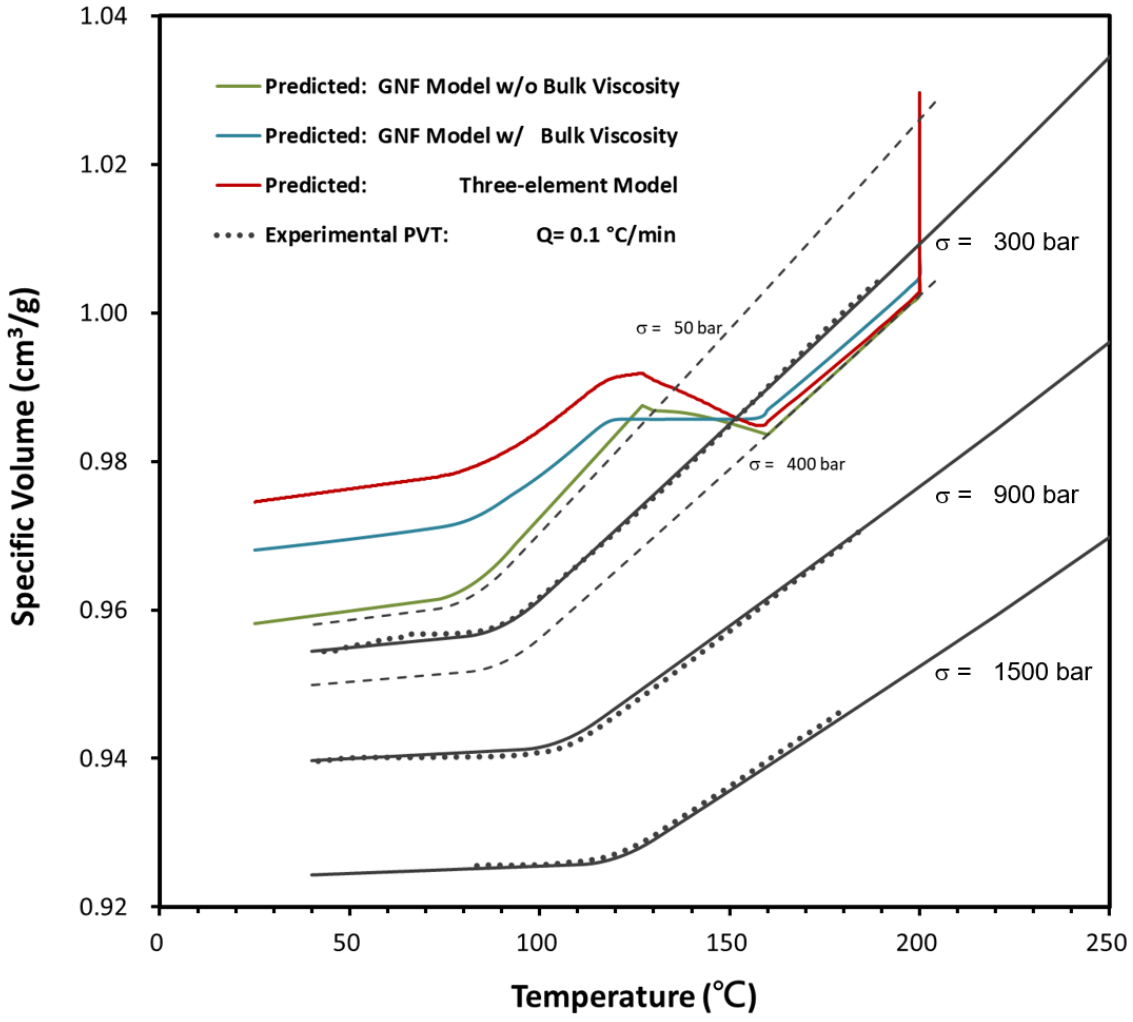

Figure 5.8 Volume evolutions with time on the PVT diagram

Table 5.3 Predicted volumetric shrinkages under the same thermal and mechanical history

Modeling	Shrinkage (%)
GNF Model w/o Bulk Viscosity	2.9
GNF Model w/ Bulk Viscosity	1.79
Three-element Model	1.65

5.9 Molding Shrinkage and Weight Predictions

Path-dependent volume evolutions predicted by models would also impact predictions of the weight and linear shrinkages of final injection molded parts. From the comparison of part weight, **Figure 5.9 (a)**, experimental weight is higher than simulations, but the three-element model has shown considerable improvement over the GNF model. For the comparison of linear shrinkage along the length direction, **Figure 5.9 (b)**, the prediction by the three-element model agrees with the experiment and shows remarkable improvement over the GNF model. From the comparison of the linear shrinkage along the width direction, **Figure 5.9 (c)**, simulations can show the increasing trend from W1 to W3, but the values are not very close to the experiment. The three-element model predicts accurate shrinkage at W3 but is less accurate at W1 and W2; a discrepancy in the prediction of cavity pressure possibly causes this. More studies, such as

considering shear viscoelasticity [60-61], could be done in the future to improve the prediction further.

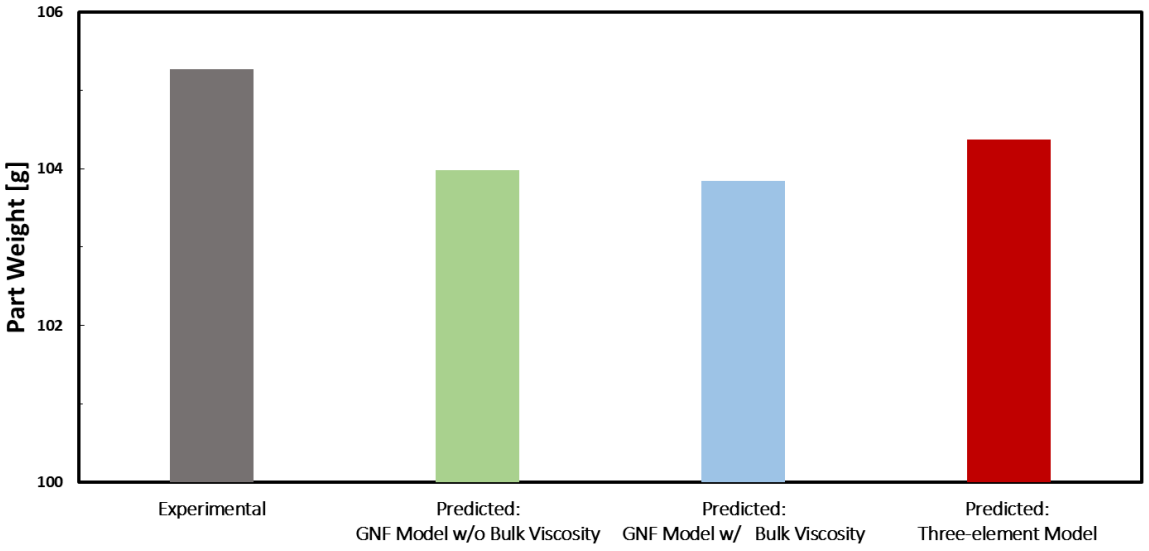

(a) Part Weight

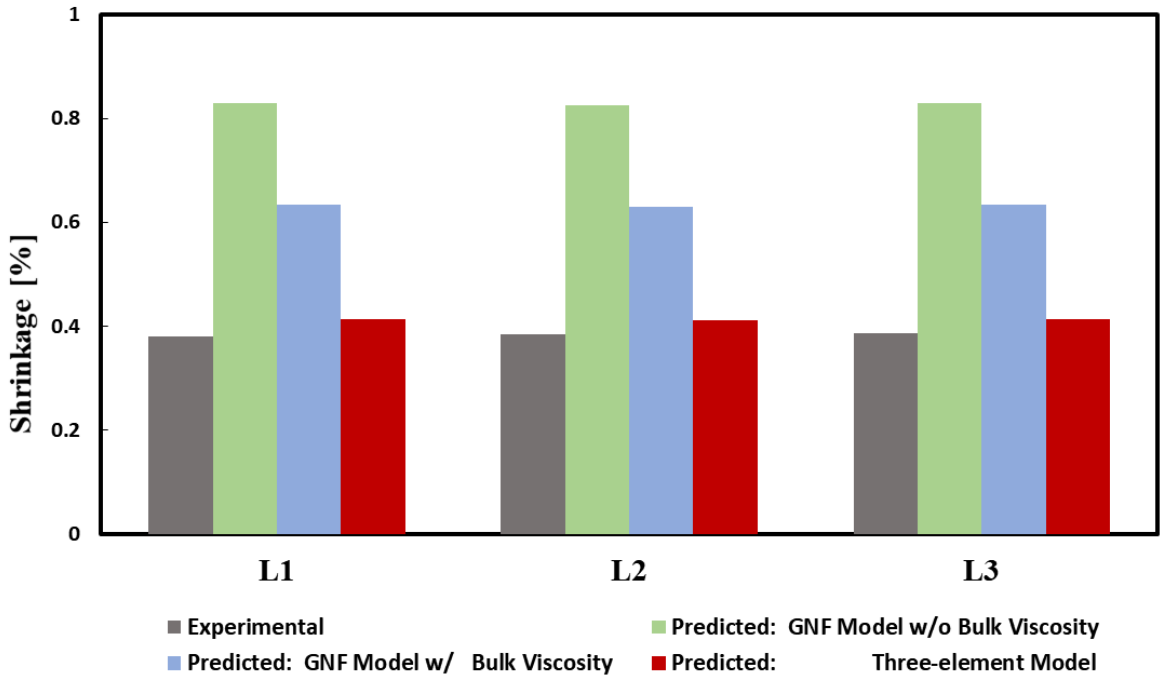

(b) Linear shrinkage in the length direction

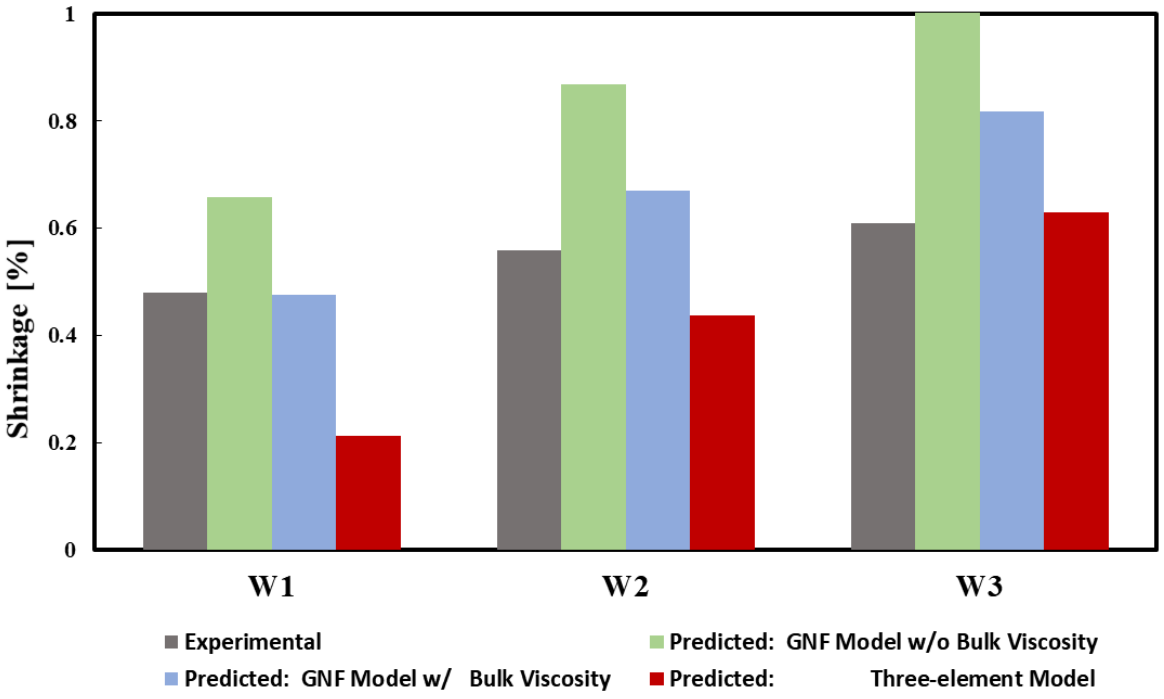

(c) Linear shrinkage in the width direction

Figure 5.9 Comparison of predictions and actual molding

6 Summary

6.1 Contributions

The full impact of bulk viscoelasticity was addressed, from measurement and model derivation, through modeling to the molding simulation. The non-equilibrium PVT obtained from cooling rate-controlled PVT measurements can be used to derive bulk viscosity. The derivation was completed by a proposed PVTQ model, which not only describes the non-equilibrium PVT experimental data well but can also extrapolate the equilibrium PVT. The derived bulk viscosity was found to be a function of temperature, pressures and rate of volume change. Followed by this experimental finding, a Cross-WLF-Arrhenius model was tested, showing capabilities of describing the bulk viscosity of the polymer melt. Results of injection molding simulation show that bulk viscoelasticity can have a considerable influence on plastic molding.

A three-element-based model was proposed in this study to describe bulk viscoelasticity better than a GNF model. This proposed model was first verified to predict isobaric cooling (cooling rate-controlled) and isothermal pressurization (bulk creep) curves on PVT diagrams with reasonable accuracy. It was later validated with an injection mold and showed significant improvements over the GNF model on predictions of cavity pressures, part weight, and linear shrinkages.

This work's results give more insight into the influence of bulk viscoelasticity during injection molding. The methodology to derive bulk viscosity from PVT measurements and the numerical approaches of considering bulk viscosity based on a flow solver can be extended to other applications or molding processes.

6.2 Recommendations for Future Work

There is still a discrepancy when comparing the predictions from the simulations and the experimental results. More studies for bulk viscoelasticity may help in reducing this discrepancy. Considering shear viscoelasticity together with bulk viscoelasticity could improve the prediction further. In addition, future work can also include the validation of more injection molds using any other amorphous polymers, measurements, and modeling of semi-crystalline polymers, as well as the influence of bulk viscoelasticity on other polymer processes.

Applying the current study on semi-crystalline polymers will be more challenging. It is possible if the crystallization effect on specific volume can be isolated from the pressure and temperature effect through experiments and considered independently in modeling. Bulk viscosity could be a function of mechanical pressure, volumetric strain rate, temperature, and relative

crystallinity. More studies in experiments and modeling should be done in the future to consider bulk viscoelasticity for semi-crystalline polymers.

6.3 Publications

The following articles detail the research products related to this dissertation:

- Y. J. Chang, R. Y. Chang, T. A. Osswald, "Measurement and modeling of bulk viscosity for polystyrene melts," Phys. Fluids, **33**, 073103 (2021).
- Y. J. Chang, R. Y. Chang, T. A. Osswald, "Modeling and simulation of bulk viscoelasticity for amorphous polymers in injection molding," Phys. Fluids, **35**, 053109 (2023)

7 Reference

[1]. T. A. Osswald, and G. Menges, Materials science of polymers for engineers (Hanser, 2012).

[2]. T. A. Osswald, (2017), Understanding polymer processing: processes and governing equations (Hanser, 2017).

[3]. Plastic Injection Molding Simulation Software Moldex3D, https://www.moldex3d.com/

[4]. J. D. Ferry, Viscoelastic properties of polymers (John Wiley & Sons, 1980).

[5]. D. W. Van Krevelen, and K. Te Nijenhuis, Properties of polymers: their correlation with chemical structure; their numerical estimation and prediction from additive group contributions (Elsevier, 2009)

[6]. A. J. Kovacs, "La contraction isotherme du volume des polymères amorphes," J. Polym. Sci., **30**, 131 (1958).

[7]. W. N. Findley, R. M. Reed, and P. Stern, "Hydrostatic creep of solid plastics," ASME. J. Appl. Mech., **34**, 895 (1967).

[8]. P. S. Theocaris, "Transient creep behaviour of crosslinked polymers in bulk deformation," Kolloid Z. Z. Polym., **236**, 59 (1970).

[9]. S. Hozumi, T. Wakabayashi, and K. Sugihara, "Volume retardation of polystyrene," Polym J, **1**, 632 (1970).

[10]. C. A. Bero, and D. J. Plazek, "Volume-dependent rate processes in an epoxy resin," J. Polym. Sci., Part B: Polym. Phys., **29**, 39 (1991).

[11]. I. Emri, and T. Prodan "A measuring system for bulk and shear characterization of polymers," Exp. Mech., **46**, 429 (2006).

[12]. Y. Meng, and S. L. Simon, "Pressure relaxation of polystyrene and its comparison to the shear response," J. Polym. Sci., Part B: Polym. Phys., **45**, 3375 (2007).

[13]. Y. Meng, P. Bernazzani, P. A. O'Connell, G. B. McKenna, and S. L. Simon, "A new pressurizable dilatometer for measuring the time-dependent bulk modulus and pressure-volume-temperature properties of polymeric materials," Rev. Sci. Instrum, **80**, 053903 (2009).

[14]. A. F. Yee, and M. T. Takemori, "Dynamic bulk and shear relaxation in glassy polymers. I. Experimental techniques and results on PMMA," J Polym Sci B Polym Phys, **20**, 205 (1982).

[15]. L. C. E. Struik, "Physical aging in plastics and other glassy materials," Polym Eng Sci., **17**, 165 (1977).

[16]. W.G. Hoover, A.J.C. Ladd, R.B. Hickman, and B.L. Holian, "Bulk viscosity via nonequilibrium and equilibrium molecular dynamics," Phys. Rev. A, **21**, 1756 (1980).

[17]. R. E. Graves, and B. M. Argrow, "Bulk viscosity: past to present," J. Thermophys. Heat Trans., **13**, 337 (1999).

[18]. S. Chen, X. Wang, J. Wang, M. Wan, H. Li, and S. Chen, "Effects of bulk viscosity on compressible homogeneous turbulence," Phys. Fluids, **31**, 085115 (2019).

[19]. F. Jaeger, O. K. Matar, and E. A. Müller, "Bulk viscosity of molecular fluids," Int. J. Chem. Phys., **148**, 174504 (2018).

[20]. S. Bhola and T. K. Sengupta, "Roles of bulk viscosity on transonic shock-wave/boundary layer interaction," Phys. Fluids, **31**, 096101 (2019).

[21]. Y. G. Ohr, "Study on the non-equilibrium temperature behavior of normal shock waves and the bulk viscosity," Phys. Fluids, **32**, 061707 (2020).

[22]. T. Chen, X. Wen, L. P. Wang, Z. Guo, J. Wang, and S. Chen, "Simulation of three-dimensional compressible decaying isotropic turbulence using a redesigned discrete unified gas kinetic scheme," Phys. Fluids, **32**, 125104 (2020).

[23]. S. Singh, M.Battiato, and R. S. Myong, "Impact of bulk viscosity on flow morphology of shock-accelerated cylindrical light bubble in diatomic and polyatomic gases," Phys. Fluids, **33**, 06610 (2021) .

[24]. B. Sharma, R. Kumar, P. Gupta, S. Pareek, and A. Singh, "On the estimation of bulk viscosity of dilute nitrogen gas using equilibrium molecular dynamics approach," Phys. Fluids, **34**, 057104 (2022).

[25]. J. P., Lesbats, R. Legros, and J. V. Aleman, "Longitudinal volume viscosity of epoxide prepolymers," J. Polym. Sci., **20**, 1971 (1982).

[26]. J. V., Aleman, "Elongational, shear and volume viscosities of polymer melts," Rheol. Acta, **27**, 238 (1988).

[27]. J. V., Aleman, "Bulk and Surface Compression Viscosities of High and Low Density Polyethylenes," Polym. Eng. Sci., **30** , 326 (1990).

[28]. P. Chivapornthip, and E. L. J. Bohez, "Dependence of bulk viscosity of polypropylene on strain, strain rate, and melt temperature," Polym. Eng. Sci., **57**, 830 (2017).

[29]. B. Kowalska, "Thermodynamic equations of state of polymers and conversion processing," Int. Polym. Sci. Technol., **29**, 76, (2002).

[30]. M. L. Wang, R. Y. Chang and C. H. Hsu, Molding simulation: Theory and practice (Hanser, 2018).

[31]. R. Zheng, R. I. Tanner, and X. J. Fan, Injection molding: integration of theory and modeling methods (Springer Science & Business Media, 2011)

[32]. W. F. Zoetelief, L. F. A. Douven, and A. I.Housz, "Residual thermal stresses in injection molded products," Polym Eng Sci., **36**, 1886 (1996).

[33]. M. R. Kamal, R. A.Lai-Fook, and J. R. Hernandez-Aguilar, "Residual thermal stresses in injection moldings of thermoplastics: a theoretical and experimental study," Polym Eng Sci., **42**, 1098 (2002).

[34]. R. Zheng, P. Kennedy, N. Phan-Thien, and X. J. Fan, "Thermoviscoelastic simulation of thermally and pressure-induced stresses in injection moulding for the prediction of shrinkage and warpage for fibre-reinforced thermoplastics," J Nonnewton Fluid Mech., **84**, 159 (1999)

[35]. K. K. Kabanemi, H. Vaillancourt, H. Wang, and G. Salloum, "Residual stresses, shrinkage, and warpage of complex injection molded products: numerical simulation and experimental validation," Polym Eng Sci., **38**, 21 (1998).

[36]. N. H. Kim, and A. I. Isayev, "Thermal birefringence in freely quenched multilayered slabs of amorphous polymers: Experiment and simulation," Polym Eng Sci., **54**, 2097 (2014).

[37]. H. Zhou, G. Xi, and F. Liu, "Residual stress simulation of injection molding," J. Mater. Eng. Perform., **17**, 422 (2008).

[38]. G. U. Losi, and W. G. Knauss, "Thermal stresses in nonlinearly viscoelastic solids," ASME. J. Appl. Mech., **59**, S43 (1992).

[39]. H. Ghoneim, and C. A. Hieber, "Incorporation of density relaxation in the analysis of residual stresses in molded parts," Polym Eng Sci., **37**, 219 (1997).

[40]. L. Grassia, and A. D'Amore, "Constitutive law describing the phenomenology of subyield mechanically stimulated glasses," Phys. Rev. E, **74**, 021504 (2006)

[41]. L. Veltmaat, F. Mehrens, H. J. Endres, J. Kuhnert, and P. Suchde, "Mesh-free simulations of injection molding processes," Phys. Fluids, **34**, 033102 (2022).

[42]. K. Krebelj, M. Halilovič, and N. Mole, "The cooling rate dependence of the specific volume in amorphous plastic injection molding", Int. J. Adv. Manuf. Technol., **103**, 1175 (2019).

[43]. Y. J. Chang, R. Y. Chang, T. A. Osswald, "Measurement and modeling of bulk viscosity for polystyrene melts," Phys. Fluids, **33,** 073103 (2021).

[44]. R. B. Bird, W. E. Stewart, and E. N. Lightfoot, Transport phenomena (John Wiley & Sons, 2006).

[45]. J.H. Dymond, and R. Malhotra, "The Tait equation: 100 years on," Int. J. Thermophy., **9** , 941 (1988).

[46]. R.Y. Chang, C.H.Chen, and K.S.Su, "Modifying the Tait equation with cooling-rate effects to predict the pressure-volume-temperature behaviors of amorphous polymers: modeling and experiments," Polym. Eng. Sci. **36**, 1789 (1996).

[47]. J. Wang, C. Hopmann, M. Schmitz, T. Hohlweck, and J. Wipperfurth, " Modeling of PVT behavior of semi-crystalline polymer based on the two-domain Tait equation of state for injection molding," Mater. Des., **183**, 108149 (2019).

[48]. R. B. Bird, R. C. Armstrong, and O. Hassager, Dynamics of polymeric liquids. Vol. 1: Fluid mechanics (John Wiley & Sons, 1987).

[49]. T. Osswald, and N. Rudolph, Polymer rheology (Hanser, 2015).

[50]. C. A. Hieber, and H. H. Chiang, "Shear-rate-dependence modeling of polymer melt viscosity," Polym. Eng. Sci., **32**, 931 (1992).

[51]. D. O. Kazmer, "System identification and modeling of viscoelastic behavior from capillary melt rheological data," Polym. Eng. Sci., **54**, 2824 (2014).

[52]. S. Raha, H. Sharma, M. Senthilmurugan, S. Bandyopadhyay and P. Mukhopadhyay, "Determination of the pressure dependence of polymer melt viscosity using a combination of oscillatory and capillary rheometer," Polym. Eng. Sci., **60**, 617 (2020).

[53]. B. Fan, and D. O. Kazmer, "Low-temperature modeling of the time-temperature shift factor for polycarbonate," Adv. Polymer. Tech., **24**, 278 (2005).

[54]. J. Capodagli, and R. Lakes, "Isothermal viscoelastic properties of PMMA and LDPE over 11 decades of frequency and time: a test of time–temperature superposition," Rheol. Acta, **47** , 777 (2008).

[55]. M. Aschenbrenner, U. Kulozik, and P. Foerst, "Evaluation of the relevance of the glassy state as stability criterion for freeze-dried bacteria by application of the Arrhenius and WLF model," Cryobiology, **65**, 308 (2012).

[56]. R. Zheng, R. I. Tanner, and X. J. Fan, Injection molding: integration of theory and modeling methods (Springer Science & Business Media, 2011).

[57]. R. Y. Chang and W. H. Yang, "Numerical simulation of mold filling in injection molding using a three-dimensional finite volume approach," Int. J. Numer. Meth. Fluids, **37**,125 (2001).

[58]. A. J. Kovacs, "Bulk creep and recovery in systems with viscosity dependent upon free volume," T. Soc, Rheol., **5**, 285 (1961).

[59]. N. Phan-Thien and N. Mai-Duy, Understanding viscoelasticity: an introduction to rheology (Springer, 2013).

[60]. E. A. Gryparis, S. D.Gkormpatsis, K. D. Housiadas, and R. I. Tanner, "Viscoelastic planar elongational flow past an infinitely long cylinder," Phys. Fluids, **31**, 033104 (2019).

[61]. H. C. Tseng, "A revisitation of White− Metzner viscoelastic fluids," Phys. Fluids, **33**, 057115 (2021).